Re-Os geochronology and coupled Os-Sr isotope constraints on the Sturtian snowball Earth

Alan D. Rooney[a,1], Francis A. Macdonald[a], Justin V. Strauss[a], Francis Ö. Dudás[b], Christian Hallmann[b,c,d], and David Selby[e]

[a]Department of Earth and Planetary Sciences, Harvard University, Cambridge, MA 02138; [b]Department of Earth, Atmospheric and Planetary Sciences, Massachusetts Institute of Technology, Cambridge, MA 02139; [c]Max-Planck-Institute for Biogeochemistry, 07745 Jena, Germany; [d]Center for Marine Environmental Sciences (MARUM), University of Bremen, 28359 Bremen, Germany; and [e]Department of Earth Sciences, Durham University, Durham DH1 3LE, United Kingdom

Edited* by Paul F. Hoffman, University of Victoria, Victoria, Canada, and approved November 8, 2013 (received for review June 21, 2013)

After nearly a billion years with no evidence for glaciation, ice advanced to equatorial latitudes at least twice between 717 and 635 Mya. Although the initiation mechanism of these Neoproterozoic Snowball Earth events has remained a mystery, the broad synchronicity of rifting of the supercontinent Rodinia, the emplacement of large igneous provinces at low latitude, and the onset of the Sturtian glaciation has suggested a tectonic forcing. We present unique Re-Os geochronology and high-resolution Os and Sr isotope profiles bracketing Sturtian-age glacial deposits of the Rapitan Group in northwest Canada. Coupled with existing U-Pb dates, the postglacial Re-Os date of 662.4 ± 3.9 Mya represents direct geochronological constraints for both the onset and demise of a Cryogenian glaciation from the same continental margin and suggests a 55-My duration of the Sturtian glacial epoch. The Os and Sr isotope data allow us to assess the relative weathering input of old radiogenic crust and more juvenile, mantle-derived substrate. The preglacial isotopic signals are consistent with an enhanced contribution of juvenile material to the oceans and glacial initiation through enhanced global weatherability. In contrast, postglacial strata feature radiogenic Os and Sr isotope compositions indicative of extensive glacial scouring of the continents and intense silicate weathering in a post–Snowball Earth hothouse.

rhenium-osmium geochronology | strontium isotopes | osmium isotopes | Windermere Supergroup | Neoproterozoic glaciation

The Snowball Earth hypothesis predicts that Neoproterozoic glaciations were global and synchronous at low latitudes and that deglaciation occurred as a result of the buildup of pCO_2 to extreme levels resulting in a "greenhouse" aftermath (1, 2). The temporal framework of Cryogenian glaciations is built on chemostratigraphy and correlation of lithologically distinct units, such as glaciogenic deposits, iron formation, and cap carbonates (3), tied to the few successions that contain volcanic rocks dated using U-Pb zircon geochronology (4). In strata lacking horizons suitable for U-Pb geochronology, Re-Os geochronology can provide depositional ages on organic-rich sedimentary rocks bracketing glaciogenic strata (5, 6). Moreover, Os isotope stratigraphy can be used as a proxy to test for supergreenhouse weathering during deglaciation (7). In a Snowball Earth scenario, we can make specific predictions for Cryogenian weathering: CO_2 consumption via silicate weathering should increase before glaciation, stagnate during the glaciation, and increase again during deglaciation. However, the use of a single weathering proxy to provide evidence for such a scenario, such as Sr isotopes from marine carbonates, is limited both by lithological constraints and an inability to distinguish between the amount of weathering and the composition of what is being weathered (8). The short residence time of Os in the present-day oceans (<10 ky) (9) provides a complementary higher resolution archive to Sr isotopes, and thus, insights into the nature of extreme fluctuations in the Earth's climate as documented herein.

Stratigraphy of the Neoproterozoic Windermere Supergroup

The Neoproterozoic Windermere Supergroup is spectacularly exposed in the Mackenzie Mountains of northwest Canada and comprises an ∼7-km-thick mixed carbonate and siliciclastic marine succession (Fig. 1 and Fig. S1). The Coates Lake Group of the Mackenzie Mountains forms the base of the Windermere Supergroup and consists of siliciclastic, carbonate, and evaporitic strata of the Thundercloud, Redstone River, and Coppercap formations. The Coates Lake Group unconformably overlies the Little Dal basalt, which has been correlated geochemically with the Tsezotene sills (10), a 777 +2.5/−1.8 Mya ($^{206}Pb/^{238}U$ multigrain zircon thermal ionization MS date) quartz diorite plug near Coates Lake (11), and the ∼780-Mya Gunbarrel magmatic event (12).

Near Coates Lake, the Coppercap Formation is ∼410 m thick and is separated into six units (CP1–CP6 in Fig. 2). The Coppercap Formation culminates with a partially dolomitized unit of carbonate conglomerate, with minor sandstone, chert, and evaporite (CP6), and is overlain by siltstone and diamictite of the Rapitan Group (Fig. 2). Economic copper deposits grading 3.9% occur in unit CP1 of the Coppercap Formation in a 1-m-thick interval (13, 14). These deposits formed directly below the flooding surface at the base of CP2 (14). Above this, in units CP2–CP5, there is no evidence for mineralization, exposure, or significant sulfate reduction, although minor evaporite and metal

Significance

The causal mechanisms of global glaciations are poorly understood. The transition to a Neoproterozoic Snowball Earth after more than 1 Gy without glaciation represents the most dramatic episode of climate change in the geological record. Here we present new Re-Os geochronology, which, together with existing U-Pb ages, reveal that the glacial period in northwest Canada lasted ∼55 My. Additionally, we present an original method to track tectonic influences on these climatic perturbations with a high-resolution coupled Os-Sr isotope curve across the transition from an ice-free world to a Neoproterozoic Snowball Earth. The data indicate that increases in mantle-derived, juvenile material emplaced onto continents and subsequently weathered into the oceans led to enhanced consumption and sequestration of CO_2 into sediments.

Author contributions: F.A.M. and J.V.S. designed research; A.D.R., F.A.M., J.V.S., F.Ö.D., and C.H. performed research; A.D.R., F.A.M., F.Ö.D., C.H., and D.S. contributed new reagents/analytic tools; A.D.R., F.A.M., J.V.S., F.Ö.D., C.H., and D.S. analyzed data; and A.D.R., F.A.M., J.V.S., F.Ö.D., and D.S. wrote the paper.

The authors declare no conflict of interest.

*This Direct Submission article had a prearranged editor.

[1]To whom correspondence should be addressed. E-mail: alanrooney@fas.harvard.edu.

This article contains supporting information online at www.pnas.org/lookup/suppl/doi:10.1073/pnas.1317266110/-/DCSupplemental.

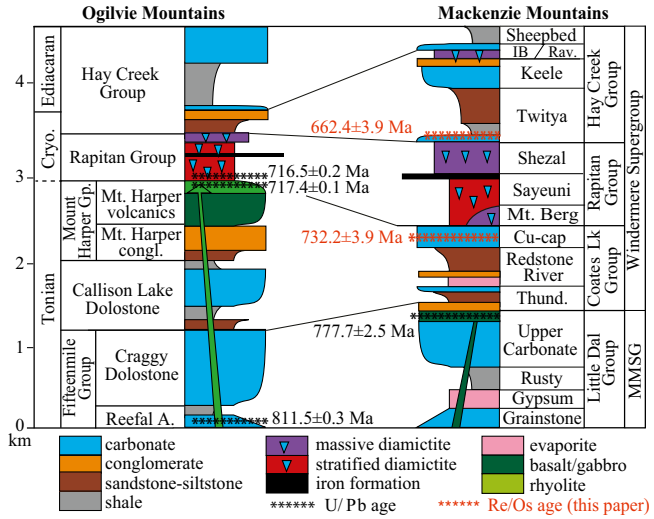

Fig. 1. Schematic of the Mackenzie and Ogilvie Mountains, Canada. U-Pb ages are from ref. 4 and Re-Os ages are from this work. Congl., conglomerate; Cryo., Cryogenian; Cu-cap, Coppercap Formation; Gp., Group; IB, Ice Brook Formation; Lk, Lake; Mt., Mount; Rav., Ravensthroat formation; Reefal A., Reefal Assemblage; Thund., Thundercloud Formation.

showings are present in association with the exposure surfaces at the top of unit CP6.

Regionally, the Rapitan Group rests unconformably on the Coates Lake Group, but locally the contact can be gradational (15). In the Ogilvie Mountains, the age of the Rapitan Group is constrained by a $^{206}Pb/^{238}U$ single grain chemical abrasion-isotope dilution-thermal ionization MS (CA-ID-TIMS) zircon date of 717.4 ± 0.1 Mya on a rhyolite from the underlying Mount Harper volcanics and 716.5 ± 0.2 Mya on a volcanic tuff within the overlying glaciogenic diamictites, indicating that glaciation commenced ~717 Mya (4). The Rapitan Group is composed of three formations consisting of stratified and massive glaciogenic diamictites with minor iron formation (16, 17). The lowest unit, the Mount Berg Formation, is present only in the southern Mackenzie Mountains. The overlying Sayunei Formation is locally more than 600 m thick and comprises ferruginous, maroon to dark brown turbiditic siltstone, sandstone, debrites, and intervals of stratified and massive glacial diamictite with dropstones of carbonate, basalt and rare granitoid clasts (16, 17). Discontinuous lenticular bodies of hematite-jaspillite iron formation are present near the top of the Sayunei Formation when they are not eroded by the overlying Shezal Formation (17, 18). The uppermost unit of the Rapitan Group, the Shezal Formation, consists of >600 m of green-gray, yellow weathering stratified and massive glacial diamictite interbedded with decameter-scale units of mudstone, siltstone and sandstone, which in some localities unconformably overlies the Sayunei Formation (11, 15, 19). Clast composition in the Shezal Formation is highly variable with an abundance of carbonate, altered basic volcanic, sandstone, chert, and less common metamorphic pebbles and cobbles (16, 17). An extended duration for deposition of the Rapitan Group is supported by internal unconformities and paleomagnetic poles that shift ~40° from the Mount Berg to Sayunei Formations (20).

Locally, the basal Twitya Formation of the Hay Creek Group conformably overlies the Rapitan Group, but regionally various parts of the Twitya Formation rest unconformably on underlying strata (19). Where conformable, such as at Mountain River, the basal Twitya Formation consists of a 0- to 40-m-thick "cap carbonate" that is characterized by finely laminated lime mudstone and siltstone with minor graded beds and sedimentary slump folds (Fig. 2). The lower Twitya Formation is part of a transgressive sequence that passes upward into fetid, pyritic black shale and then into hundreds of meters of gray-green siltstone and sandstone turbidites. These strata are succeeded by variable siliciclastic and carbonate strata of the Keele Formation and glaciogenic deposits of the Stelfox Member of the Ice Brook Formation. The Stelfox Member consists of massive diamictite with striated clasts (21) and is capped by the Ravensthroat formation, a white to buff-colored dolostone (17, 22), which hosts sedimentological and geochemical features characteristic of globally distributed ~635 Mya Marinoan cap carbonates (2, 23).

Re-Os Geochronology

Organic-lean (<0.5% Total Organic Carbon; TOC) cryptalgal laminites of the Coppercap Formation were obtained from drill core and outcrop near Coates Lake (Figs. 1 and 2). Core samples were analyzed for major and minor elements, carbonate content, and C, Sr, and Os isotope chemostratigraphy, and four samples were used for Re-Os geochronology and Os isotope stratigraphy (see *SI Materials and Methods* for details).

A Re-Os age of 732.2 ± 3.9 Mya [4.7 Mya including ^{187}Re decay constant uncertainty, n = 4, mean square of weighted deviates (MSWD) = 1.9, 2σ, initial $^{187}Os/^{188}Os$ = 0.15 ± 0.002] was obtained from unit CP4 of the Coppercap Formation (Fig. 3*A*). In conjunction with existing U-Pb zircon ages from the Ogilvie Mountains, this Re-Os age indicates an interval ~15 My

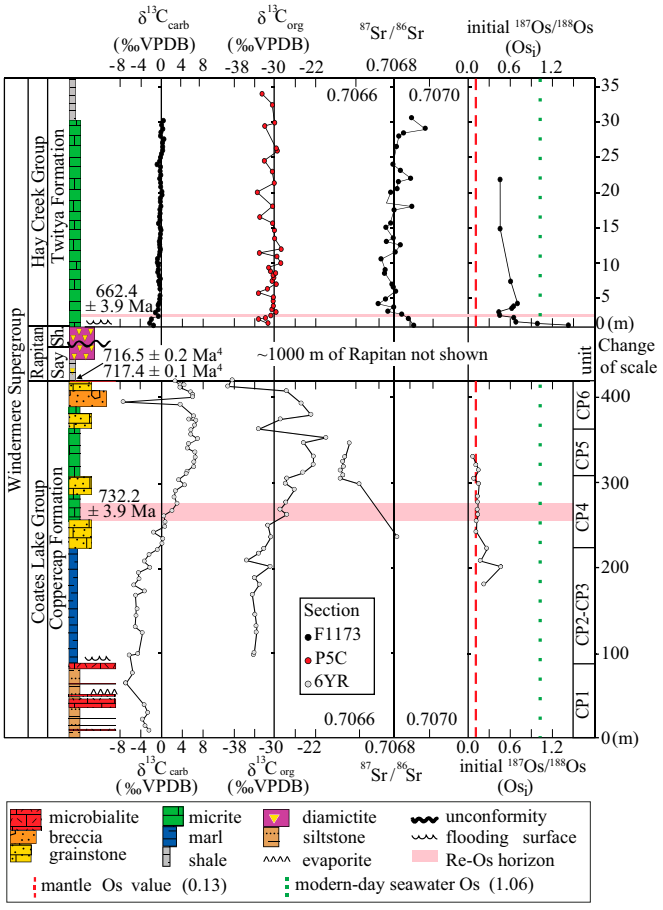

Fig. 2. Composite chemo- and lithostratigraphy of the Windermere Supergroup from the Mackenzie Mountains, Canada (measured sections F1173, P5C, and 6YR). Organic carbon isotope data for the Twitya Formation in Section P5C is from ref. 24. Say, Sayunei; Sh, Shezal. The superscript next to 716 and 717 Ma corresponds to the cited reference.

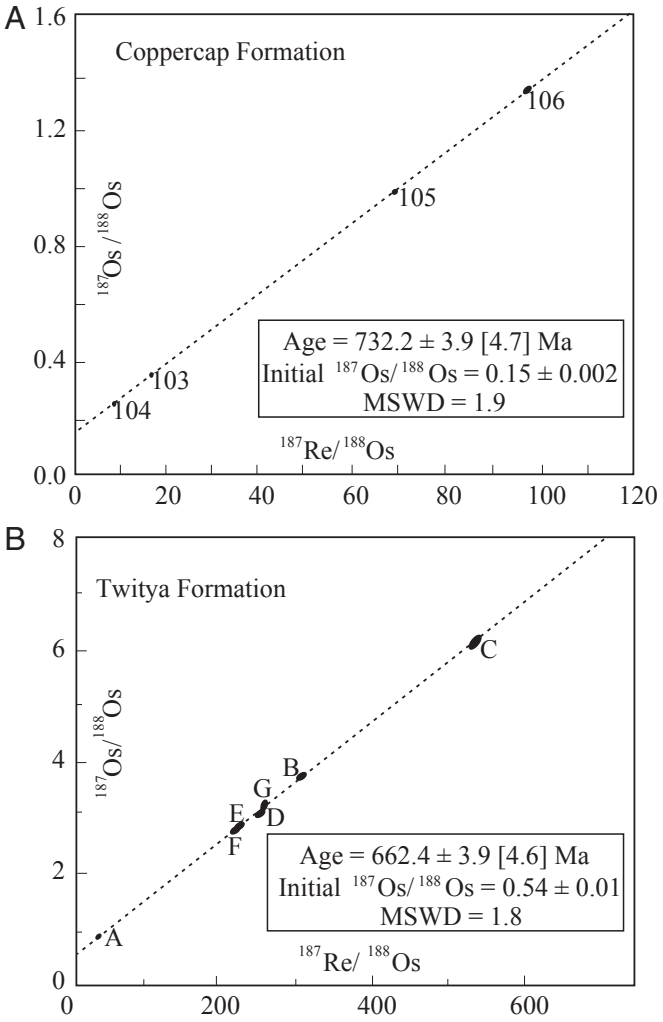

Fig. 3. (*A*) Re-Os isochron for the Coppercap Formation with an age uncertainty of 4.7 Mya when the uncertainty in the ^{187}Re decay constant is included. (*B*) Re-Os isochron for the Twitya Formation with an age uncertainty of 4.6 Mya when the uncertainty in the ^{187}Re decay constant is included. Isotope composition and abundance data are presented in Table S2.

between deposition of unit CP4 of the Coppercap Formation and Rapitan Group glaciogenic strata (Figs. 1 and 2).

Organic-rich (>0.5% TOC) micritic limestone of the post-glacial basal Twitya Formation was sampled from outcrop near Mountain River (64°32′04″N, 129°23′42″W). The cap limestone was sampled at ~0.5-m resolution for Sr, Os, and C isotope chemostratigraphy (24), and a thin (<20 cm) horizon less than 2 m above the Rapitan-Twitya contact was sampled for Re-Os geochronology (Fig. 2). The basal Twitya Formation yielded a Re-Os age of 662.4 ± 3.9 Mya (4.6 Mya including ^{187}Re decay constant uncertainty, $n = 7$, MSWD = 1.9, 2σ, initial ^{187}Os/^{188}Os = 0. 54 ± 0.01; Fig. 3*B*). The 662.4 ± 3.9 Mya Re-Os date for the Twitya Formation together with the CA-ID-TIMS zircon date of 716.5 ± 0.2 Mya from the nearby Ogilvie Mountains (4) represents a crucial set of age constraints that date both the onset and demise of a Cryogenian glaciation from the same continental margin. Correlation of the Rapitan Group from the Yukon to the Northwest Territories (NWT) is supported not only by the bracketing stratigraphy but also by the presence of iron formation (25, 26) and paleomagnetic studies that link Rapitan poles from the NWT with the 723–716 Mya Franklin large igneous province (20, 27), which was coeval with Rapitan glaciation in the Yukon (4).

Coupled Os and Sr Isotope Stratigraphy

The Os and Sr isotope compositions of seawater have been interpreted to reflect an input balance between radiogenic sources (weathering of upper continental crust and riverine input) and unradiogenic sources (cosmic dust, hydrothermal alteration of oceanic crust, and weathering of mafic or ultramafic rocks) (28). However, Os and Sr have distinct sources and sinks, are sensitive to varying geological processes, and have contrasting residence times. Therefore, combining these two weathering proxies to investigate Neoproterozoic climatic fluctuations represents a unique method to elucidate the relationship between increased rates of continental weathering and global climate change.

Initial ^{187}Os/^{188}Os (Os_i) values from the preglacial Coppercap Formation become increasingly unradiogenic up-section from a value of 0.24 to a nadir of 0.12 before Rapitan Group deposition (Fig. 2). This extremely low Os_i value is substantially less radiogenic than values reported for modern seawater (^{187}Os/^{188}Os = 1.06) (28) and is closer to the primitive upper mantle Os isotope composition (732 Mya = ^{187}Os/^{188}Os = 0.124) (29). Although it is possible that episodic restriction within the Coates Lake basin, potential hydrothermal input, and/or weathering of a proximal ultramafic body may have contributed to the unradiogenic Os_i values in the Coppercap Formation (Fig. 2), units CP2–CP6 have been previously interpreted to have been deposited in an open marine embayment (14, 30).

In the Coppercap Formation, Sr isotope values are extremely scattered in units CP1–CP3 between 0.7169 and 0.7064, less scattered in units CP4 and CP5 with values converging between 0.7064 and 0.7066, and scattered again in unit CP6. In the Twitya Formation, Sr isotope values decline from 0.7069 to 0.7067 in the basal 5 m and continue to oscillate between 0.7068 and 0.7070 over the ensuing 20 m (Fig. 2 and Table S1).

Unlike the Phanerozoic marine Sr isotope curve, whose fidelity can be evaluated by comparisons between several sample types (31), Neoproterozoic marine Sr chemostratigraphy relies exclusively on analyses of whole rock carbonate samples that have potentially been subjected to a variety of diagenetic processes. Based on data from sequential dissolution experiments (32), Sr isotopic analyses of whole rock carbonate samples can be expected to vary in the fourth decimal place, i.e., the external reproducibility of "replicates" from the same sample is ±0.0001. Sr isotope measurements are commonly vetted for reliability with Mn/Sr, Sr/Ca, Rb/Sr, and Sr concentration. Mn/Sr is thought to be a sensitive indicator of alteration due to the increase in Mn and decrease of Sr during meteoric alteration (33, 34); however, we find that Mn/Sr and Rb/Sr ratios scale inversely with carbonate content (Table S1), likely reflecting the contamination of small amounts of Sr from clay minerals. Consequently, we cull unreliable results with both low carbonate content and Sr abundance. Above 90% carbonate content and Sr concentrations >650 ppm, ^{87}Sr/^{86}Sr scatter above 0.708 is eliminated. However, for samples with 87Sr/86Sr between 0.7064 and 0.7080 there is no dependence on carbonate content, Sr concentration, Mn/Sr, Rb/Sr, or Sr/Ca (Table S1). The lowest and most stratigraphically coherent and reproducible values are in units CP4 and CP5 and in the Twitya Formation. We thus consider these ^{87}Sr/^{86}Sr measurements as the most reliable (Fig. 2 and Table S1).

The lower Coppercap Formation (units CP1–CP3) contains detrital components derived from the Little Dal Basalt and siliciclastic strata of the Katherine Group (14). These strata have also been geochemically modified by basin-dewatering brines that were responsible for formation of the Coates Lake sediment-hosted Cu deposit. We interpret the radiogenic ^{87}Sr/^{86}Sr of the lower Coppercap Formation to reflect effects of both

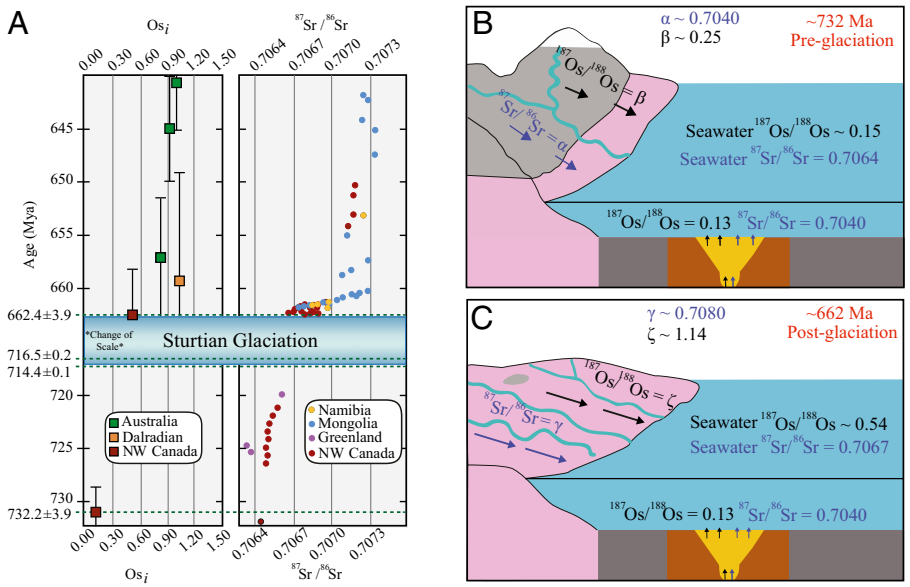

Fig. 4. (*A*) Compilation of initial ^{187}Os/^{188}Os isotope data and ^{87}Sr/^{86}Sr data for pre- and post-Sturtian successions worldwide (5, 6, 40, 53, 70). All data are in Tables S1–S5. (*B*) Geological cartoon of Neoproterozoic preglacial weathering fluxes. (*C*) Geological cartoon of postglacial weathering fluxes. See text and *SI Materials and Methods* for further details.

a higher siliciclastic component and potential postdepositional modification by basin-dewatering brines.

Duration and Synchronicity of the Sturtian Glacial Epoch

The Twitya Formation Re-Os date is identical, within uncertainty, to existing postglacial U-Pb zircon geochronological data from Australia and South China (Fig. 4, Fig. S2, and Table S6) (35, 36), although there are some discrepancies related to analytical procedures of some of the Re-Os ages from Australia (5, 6). Previous work yielded Re-Os age constraints for the Tindelpina Formation (6), which is an amalgamated date based on Re-Os data from two separate drill cores (SCYW-1a and Blinman-2) separated by >100 km. These two horizons were correlated using low-resolution δ^{13}C stratigraphy, which is not an accurate technique for sample selection for Re-Os geochronology. The four-point SCYW1a isochron in their study (6) contains two data points (a3-4 and a3-4r; Table S5) (supplemental data of ref. 6) that are actually two analyses of a single sample suggesting extreme sample heterogeneity. Due to these complications, we consider the SCYW1a age to be misleading and not suitable for global correlation.

A Re-Os date of 640.7 ± 4.7 Mya from Tasmanian organic-rich rocks has also been used to dispute the synchronicity of the Rapitan-Sturtian deglaciation (5). However, this date from the upper Black River Formation is located stratigraphically above two diamictite units that are separated by a carbonate unit and is overlain by the ~580-Mya Gaskiers-age Croles Hill diamictite (37). The Croles Hill diamictite was previously correlated with the Marinoan Cottons Breccia on King Island and the Elatina Formation in the Flinders Range of Australia, which implied that the upper Black River Formation was Sturtian in age. However, a new ^{206}Pb/^{238}U zircon CA-ID-TIMS date of 636.41 ± 0.45 Mya from the Cottons Breccia (23) suggests that the 640.7 ± 4.7-Mya Re-Os age in the upper Black River Formation is instead correlative with the ~635-Mya Marinoan glaciation.

The glaciogenic Port Askaig Formation of the Dalradian Supergroup, Scotland, was deposited on the northeast margin of Laurentia and has been correlated with the Sturtian glaciation using lithostratigraphic and chemostratigraphic techniques (38, 39). A Re-Os age of 659.6 ± 9.6 Mya for the Ballachulish Slate near Loch Leven (40) has been cited as a maximum age constraint for the Port Askaig Formation; however, the Port Askaig is not present in the region, and the relationship of the date to glacigenic strata relies on regional correlations. A variety of tests on samples from the Ballachulish Slate indicate that the 659.6 ± 9.6-Mya age represents a depositional age and not a mixed age from later metamorphic events (40). Therefore, if we assume that the ages on the Ballachulish and Twitya formations are robust, we are left with the following alternatives: (*i*) these dates are constraining two separate glaciations during the "Sturtian glacial epoch," and these ages bracket the later event; (*ii*) the Sturtian glaciation is not preserved on the eastern margin of Laurentia, and the Port Askaig Formation represents the younger (~635 Mya) Marinoan glaciation and is correlative with the Stralinchy diamictite; or (*iii*) the Kinlochlaggan Boulder Bed is correlative with the Port Askaig Tillite as originally suggested by refs. 41 and 42. As a result, the Ballachulish Slate near Loch Leven would lie in the Argyll Group. Ultimately, additional tests of regional correlations and geochronological constraints are necessary to more fully resolve the complexities of the Dalradian Supergroup.

Existing ^{206}Pb/^{238}U zircon ages from Idaho have been previously used to argue that the Sturtian glaciation is globally diachronous (43, 44). However, these ages, coupled with the 711.5 ± 0.3-Mya age from the Gubrah Formation in Oman (45), can also be interpreted to be syn-glacial constraints and correlative with the 717- to 662-Mya Sturtian glacial epoch recorded in northwest Canada (Fig. 4). Additional constraints from U-Pb and Re-Os geochronology are necessary to determine whether Sturtian glacial strata represent a series of glacial–interglacial cycles (46), a Jormagund climate state (47), or a continuous ~55-My Snowball Earth event.

It has also been suggested that there was an earlier, ~750-Ma glaciation recorded on the Kalahari (48), Congo (49), and Tarim (50) cratons. However, there is no direct evidence for glaciation in Kaigas Formation on the Kalahari Craton (51), and the ages from the Congo and Tarim cratons suffer from inheritance and cannot be relied on (see concordia diagrams in refs. 49 and 50). Our Re-Os age of 732.2 ± 3.9 Mya on the Coppercap Formation coupled with global C and Sr isotope correlation is consistent

with the lack of evidence for a pre-717-Mya glaciation. The large negative carbon isotope anomaly in the lower Coppercap Formation covaries in carbonate carbon and organic carbon isotopes (Fig. 2) and can be correlated with the Islay anomaly in Scotland, Greenland, and Svalbard (3). It is also consistent with pre-Sturtian Sr isotope values (52, 53). However, the Islay anomaly in Scotland is not present in the Loch Leven region in Scotland, and its relationship to the dated Ballachulish Slate (40) is unclear. The Re-Os geochronology presented here suggests that the Islay anomaly returns to positive $\delta^{13}C_{carb}$ values by ~732 Mya, well before the onset of glaciation at ~717 Mya (4). Therefore, this anomaly cannot be mechanistically linked to the onset of glaciation as has been previously proposed (54–56). Moreover, none of these successions host any evidence for glaciation before the Islay anomaly.

Fire and Ice Revisited

The Sr isotope data reported here at ~732 Ma—as low as ~0.7064 in the Coppercap Formation—are consistent with other low pre-Sturtian values recorded in strata from Svalbard and Greenland (52, 53) and are less radiogenic then the ~780-Mya values from Svalbard (57). Interestingly, Nd isotope studies have also suggested an increase to more mantle-like (more radiogenic) values tens of millions of years before the Sturtian glaciation (57). These data are consistent with the Fire and Ice hypothesis (58, 59), which proposes that Cryogenian glaciations were initiated through enhanced CO_2 consumption via weathering of basalts emplaced at low latitudes. The low-latitude breakup of Rodinia is thought to have been associated with the development of juvenile volcanic rift margins and the emplacement of multiple large igneous provinces (e.g., Willouran, Guibei, Gunbarrel, and Franklin large igneous provinces) (60). Enhanced volcanism and weathering of mafic material would have driven the ocean towards more unradiogenic Sr values and mantle-like Os_i values and a cooler global climate (Fig. 4), analogous to scenarios proposed for Mesozoic ocean anoxic events and Cenozoic cooling episodes (61–63).

In sharp contrast, the Os_i data from the overlying Twitya Formation yield a radiogenic signal for the postglacial ocean with the basal cap limestone recording an Os_i value of 1.44. From this initial high, values decline rapidly reaching a nadir of 0.42 at a height 2.6 m above the diamictite and then become steadily more radiogenic to a value of 0.62 before stabilizing to values ~0.50 above 10 m (Fig. 2). Similarly, Sr isotope values decrease from 0.7068 to 0.7066 in the lower 3 m and continue to fluctuate up-section before leveling out between 0.7068 and 0.7070. We interpret the signal recorded in the lower 3 m to represent the highly radiogenic, unmixed glacial melt water plume (64) and a subsequent decrease to less radiogenic Sr isotope values at 3–10 m to reflect the transgression of glacial deep waters (65). Up-section, it appears as though rapid mixing obscures the melt water signal; however, enhanced silicate weathering continued through the transgression in a high pCO_2 environment, resulting in an Os_i much more radiogenic than preglacial values, complementing the radiogenic trend recorded in the coeval Sr composition of seawater (Fig. 2). The absence of a trend to unradiogenic Sr isotope values across Cryogenian glacial deposits led some workers to conclude that Neoproterozoic glaciations were short lived (<1 My) (66). However, this approach neglects carbonate dissolution in response to ocean acidification and assumes that the Sr cycle is in steady state (67, 68), which is inconsistent with the sharp rise seen in globally distributed cap carbonate deposits.

Sr isotope data from Sturtian cap limestones in Namibia, Mongolia, and northwest Canada agree to the fourth decimal place (69, 70), thereby supporting a global correlation of this trend (Fig. 4). These Sr values increase rapidly from 0.7066 to 0.7072 in the Sturtian cap carbonate sequence and then flat-line through the rest of the Cryogenian period. Thus, the Neoproterozoic rise in seawater Sr isotope values may not have been gradual, as previously suggested (52), but stepwise and driven by extreme weathering in a postglacial supergreenhouse.

Conclusions

The geological record suggests that the Earth's climate system can exist in two climatic equilibria: one globally glaciated and the other not (46, 47). However, both the processes that maintain a steady climate and the drivers of long-term (>10 My) climate change have remained obscure. Following a billion years of relative climatic stability with no apparent glacial deposits, the Neoproterozoic witnessed the transition from an ice-free world to a Snowball Earth. The unique Os and Sr isotope stratigraphy coupled with the Re-Os geochronology data presented herein also point towards a tectonic driver for long-term climate change and that the change in global weatherability may have been driven by a relative increase in juvenile, mantle-derived material weathered into the oceans from the continents.

Initiation of a Snowball Earth through a change in global weatherability has been criticized on the grounds that these background conditions should have persisted on a >10-My timescale, and after deglaciation the Earth should have rapidly returned to a Snowball state (46). Our new constraint of an ~55-My duration of the Sturtian glacial epoch in northwest Canada is consistent with a short interlude between the Sturtian and Marinoan glaciations and a return to a glacial state on a timescale consistent with enhanced weatherability (71). Increased input of mantle-derived material to the ocean would have also influenced geochemical cycles and promoted anaerobic respiration, potentially providing additional feedbacks that conspired to initiate a Neoproterozoic Snowball Earth (54). Our results confirm that the Sturtian glacial epoch was long lasting, its onset was accompanied by basalt-dominated weathering, and its termination was globally synchronous and followed by extreme weathering of the continents. The post-Sturtian weathering event may have in turn provided limiting nutrients like phosphorous to the ocean (72), leading to an increase in atmospheric oxygen and the radiation of large animals with high metabolic demands.

ACKNOWLEDGMENTS. We thank Rigel Lustwerk for providing samples from the 6YR core. We are grateful to the Yukon Geological Survey, Roger Summons, and Massachusetts Institute of Technology's National Aeronautics and Space Administration Astrobiology Institute node for support. We thank Roger Summons, Sam Bowring, and Dan Schrag for the use of their laboratories. We acknowledge the superb teams at Canadian and Fireweed helicopter companies and Dugald Dunlop from Meridian Mining via Colorado Minerals. We thank three reviewers and Paul Hoffman for comments on the manuscript and editorial advice. The Durham Laboratory for Source Rock Geochronology and Geochemistry is partially funded by TOTAL and BP. C.H. was supported by the Agouron Institute.

1. Hoffman PF, Kaufman AJ, Halverson GP, Schrag DP (1998) A neoproterozoic snowball earth. *Science* 281(5381):1342–1346.
2. Hoffman PF, Schrag DP (2002) The snowball Earth hypothesis; testing the limits of global change. *Terra Nova* 14(3):129–155.
3. Halverson GP, Hoffman PF, Schrag DP, Maloof AC, Rice AHN (2005) Toward a Neoproterozoic composite carbon-isotope record. *Geol Soc Am Bull* 117(9-10):1181–1207.
4. Macdonald FA, et al. (2010) Calibrating the Cryogenian. *Science* 327(5970):1241–1243.
5. Kendall BS, Creaser RA, Calver CR, Raub TD, Evans DAD (2009) Correlation of Sturtian diamictite successions in southern Australian and northwestern Tasmania by Re-Os black shale geochronology and the ambiguity of "Sturtian"-type diamictite-cap carbonate pairs as chronostratigraphic marker horizons. *Precambrian Res* 172:301–310.
6. Kendall BS, Creaser RA, Selby D (2006) Re-Os geochronology of postglacial black shales in Australia: Constraints on the timing of "Sturtian" glaciation. *Geology* 34:729–732.
7. Ravizza G, Peucker-Ehrenbrink B (2003) The marine $^{187}Os/^{188}Os$ record of the Eocene-Oligocene transition: The interplay of weathering and glaciation. *Earth Planet Sci Lett* 210:151–165.
8. Raymo ME, Ruddiman WF (1992) Tectonic forcing of late Cenozoic climate. *Nature* 359:117–122.

9. Paquay FS, Ravizza G (2012) Heterogeneous seawater $^{187}Os/^{188}Os$ during the Late Pleistocene glaciations. *Earth Planet Sci Lett* 349:126–138.
10. Dudás FO, Lustwerk RL (1997) Geochemistry of the Little Dal basalts: Continental tholeiites from the Mackenzie Mountains, Northwest Territories, Canada. *Can J Earth Sci* 34:50–58.
11. Jefferson CW, Parrish R (1989) Late Proterozoic stratigraphy, U/Pb zircon ages and rift tectonics, Mackenzie Mountains, northwestern Canada. *Can J Earth Sci* 26:1784–1801.
12. Harlan SS, Heaman LM, LeCheminant AN, Premo WR (2003) Gunbarrel mafic magmatic event: A key 780 Ma time marker for Rodinia plate reconstructions. *Geology* 31: 1053–1056.
13. Chartrand FM, Brown AC (1985) The diagenetic origin of stratiform copper mineralization, Coates Lake, Redstone Copper belt, NWT, Canada. *Econ Geol* 80:325–343.
14. Lustwerk RL (1990) Geology and geochemistry of the Redstone strataform copper deposit, Northwest Territories, Canada. PhD thesis (Pennsylvania State Univ, University Park, PA).
15. Helmstaedt H, Eisbacher GH, McGregor JA (1979) Copper mineralization near an intra-Rapitan unconformity, Nite copper prospect, Mackenzie Mountains, Northwest Territories, Canada. *Can J Earth Sci* 16:50–59.
16. Eisbacher GH (1978) *Redefinition and Subdivision of the Rapitan Group, Mackenzie Mountains* (Geological Survey of Canada, Ottawa), pp 1–21.
17. Hoffman PF, Halverson GP (2011) Neoproterozoic glacial record in the Mackenzie Mountains, northern Canadian Cordillera. *The Geological Record of Neoproterozoic Glaciations*, eds Arnaud E, Halverson GP, Shields-Zhou G (The Geological Society, London), Vol 36, pp 397–412.
18. Klein C, Beukes NJ (1993) Sedimentology and geochemistry of the glaciogenic late Proterozoic Rapitan iron-formation in Canada. *Econ Geol* 84:1733–1774.
19. Eisbacher GH *Sedimentary Tectonics and Glacial Record in the Windermere Supergroup, Mackenzie Mountains, Northwestern Canada* (Geological Survey of Canada, Ottawa), pp 1–40.
20. Park JK (1997) Paleomagnetic evidence for low-latitude glaciation during deposition of the Neoproterozoic Rapitan Group, Mackenzie Mountains, N.W.T., Canada. *Can J Earth Sci* 34:34–49.
21. Aitken JD (1991) *The Ice Brook Formation and Post-Rapitan, Late Proterozoic glaciation, Mackenzie Mountains, Northwest Territories* (Geological Survey of Canada, Ottawa), Vol 404, pp 1–43.
22. James NP, Narbonne GM, Kyser TK (2001) Late Neoproterozoic cap carbonates: Mackenzie Mountains, northwestern Canada: Precipitation and global glacial meltdown. *Can J Earth Sci* 38(8):1229–1262.
23. Calver CR, et al. (2013) Globally synchronous Marinoan deglaciation indicated by U-Pb geochronology of the Cottons Breccia, Tasmania, Australia. *Geology* 41:1127–1130.
24. Johnston DT, Macdonald FA, Gill BC, Hoffman PF, Schrag DP (2012) Uncovering the Neoproterozoic carbon cycle. *Nature* 483(7389):320–323.
25. Young GM (1976) Iron-formation and glaciogenic rocks of the Rapitan Group, Northwest Territories, Canada. *Precambrian Res* 3:137–158.
26. Young GM (1982) The late Proterozoic Tindir Group, east-central Alaska; Evolution of a continental margin. *Geol Soc Am Bull* 93:759–783.
27. Denyszyn SW, Halls HC, Davis DW, Evans DAD (2009) Paleomagnetism and U-Pb geochronology of Franklin dykes in High Arctic Canada and Greenland: A revised age and paleomagnetic pole for constraining block rotations in the Nares Strait region. *Can J Earth Sci* 46:689–705.
28. Peucker-Ehrenbrink B, Ravizza G (2000) The marine osmium isotope record. *Terra Nova* 12:205–219.
29. Meisel T, Walker RJ, Irving AJ, Lorand J-P (2001) Osmium isotopic compositions of mantle xenoliths: A global perspective. *Geochim Cosmochim Acta* 65:1311–1323.
30. Jefferson CW (1978) *The Upper Proterozoic Redstone Copper Belt, Mackenzie Mountains, Northwest Territories. PhD thesis* (Univ of Western Ontario, London, Canada).
31. Brand U (2004) Carbon, oxygen and strontium isotopes in Paleozoic carbonate components: An evaluation of original seawater-chemistry proxies. *Chem Geol* 204:23–44.
32. Li D, Shields-Zhou G, Ling HF, Thirwall M (2011) Dissolution methods for strontium isotope stratigraphy: Guidelines for the use of bulk carbonate and phosphorite rocks. *Chem Geol* 290:133–144.
33. Derry LA, Keto LS, Jacobsen SB, Knoll AH, Swett K (1989) Sr isotopic variations in Upper Proterozoic carbonates from Svalbard and East Greenland. *Geochim Cosmochim Acta* 53(9):2331–2339.
34. Banner JL, Hanson GN (1990) Calculation of simultaneous isotopic and trace element variations during water-rock interaction with application to carbonate diagenesis. *Geochim Cosmochim Acta* 54:3123–3137.
35. Fanning CM, Link PK (2008) Age constraints for the Sturtian glaciation: Data from the Adelaide Geosyncline, South Australia and Pocatello Formation Idaho, USA. *Neoproterozoic extreme climates and the origin of early metazoan life*, eds Gallagher SJ, Wallace MW. *Selwyn Symposium* (Geological Society of Australia), pp 57–62.
36. Zhou C, et al. (2004) New constraints on the ages of Neoproterozoic glaciations in south China. *Geology* 32:437–440.
37. Calver CR, Black LP, Everard JL, Seymour DB (2004) U-Pb zircon age constraints on late Neoproterozoic glaciation in Tasmania. *Geology* 32(10):893–896.
38. Brasier MD, Shields G (2000) Neoproterozoic chemostratigraphy and correlation of the Port Askaig glaciation, Dalradian Supergroup of Scotland. *J Geol Soc London* 157: 909–914.
39. Prave AR, Fallick AE, Thomas CW, Graham CM (2009) A composite C-isotope profile for the Neoproterozoic Dalradian Supergroup of Scotland and Ireland. *J Geol Soc London* 166:1–13.
40. Rooney AD, Chew DM, Selby D (2011) Re-Os geochronology of the Neoproterozoic-Cambrian Dalradian Supergroup of Scotland and Ireland: Implications for Neoproterozoic stratigraphy, glaciation and Re-Os systematics. *Precambrian Res* 185:202–214.
41. Treagus JE (1969) The Lower Dalradian Kinlochlaggan Boulder Bed, central Scotland. *Earth Pre-Pleistocene Glacial Record*, eds Hambrey MJ, Harland WB (Cambridge Univ Press, Cambridge, UK), pp 637–639.
42. Evans RHS, Tanner PWG (1996) A late Vendian age for the Kinlochlaggan Boulder Bed (Dalradian)? *J Geol Soc London* 153:823–826.
43. Fanning CM, Link PK (2004) U-Pb SHRIMP ages of Neoproterozoic (Sturtian) glaciogenic Pocatello Formation, southeastern Idaho. *Geology* 32:881–884.
44. Keeley JA, Link PK, Fanning CM, Schmitz MD (2013) Pre- to synglacial rift-related volcanism in the Neoproterozoic (Cryogenian) Pocatello Formation, SE Idaho: New SHRIMP and CA-ID-TIMS constraints. *Lithosphere* 5(1):128–150.
45. Bowring SA, Grotzinger JP, Condon DJ, Ramezani J, Newall M (2007) Geochronologic constraints on the chronostratigraphic framework of the Neoproterozoic Huqf Supergroup, Sultanate of Oman. *Am J Sci* 307:1097–1145.
46. Pierrehumbert RT, Abbot DS, Voigt A, Koll D (2011) Climate of the Neoproterozoic. *Annu Rev Earth Planet Sci* 39:417–460.
47. Abbot DS, Voigt A, Koll D (2011) The Jormungand global climate state and implications for Neoproterozoic glaciations. *J Geophys Res* 116(D18103).
48. Frimmel HE, Klotzli US, Siegfried PR (1996) New Pb-Pb single zircon age constraints on the timing of Neoproterozoic glaciation and continental break-up in Namibia. *J Geol* 104:459–469.
49. Key RM, et al. (2001) The western arm of the Lufilian Arc in NW Zambia and its potential for copper mineralization. *J Afr Earth Sci* 33:503–528.
50. Xu B, et al. (2009) SHRIMP zircon U-Pb age constraints on Neoproterozoic Quruqtagh diamictites in NW China. *Precambrian Res* 168:247–258.
51. Macdonald FA, Strauss JV, Rose CV, Dudás FO, Schrag DP (2010) Stratigraphy of the Port Nolloth Group of Namibia and South Africa and implications for the age of Neoproterozoic iron formations. *Am J Sci* 310:862–888.
52. Halverson GP, Dudás FO, Maloof AC, Bowring SA (2007) Evolution of the $^{87}Sr/^{86}Sr$ composition of Neoproterozoic seawater. *Palaeogeogr Palaeoclimatol Palaeoecol* 256:103–129.
53. Fairchild IJ, Spiro B, Herrington PM, Song T (2000) Controls on Sr and C isotope compositions of Neoproterozoic Sr-rich limestones of East Greenland and North China. *Carbonate Sedimentation and Diagenesis in the Evolving Precambrian World*, eds Grotzinger JP, James NP (SEPM Special Publication, Tulsa, OK), Vol 67, pp 297–313.
54. Tziperman E, Halevy I, Johnston DT, Knoll AH, Schrag DP (2011) Biologically induced initiation of Neoproterozoic snowball-Earth events. *Proc Natl Acad Sci USA* 108(37): 15091–15096.
55. Hoffman PF, et al. (2012) Cryogenian glaciations on the southern tropical paleomargin of Laurentia (NE Svalbard and East Greenland), and a primary origin for the upper Russoya (Islay) carbon isotope excursion. *Precambrian Res* 206-207:137–158.
56. Schrag DP, Berner RA, Hoffman PF, Halverson GP (2002) On the initiation of snowball Earth. *Geochem Geophys Geosyst* 3(6).
57. Halverson GP, Wade BP, Hurtgen MT, Barovich KM (2010) Neoproterozoic Chemostratigraphy. *Precambrian Res* 182(4):337–350.
58. Donnadieu Y, Goddéris Y, Ramstein G, Nédélec A, Meert J (2004) A 'snowball Earth' climate triggered by continental break-up through changes in runoff. *Nature* 428(6980):303–306.
59. Godderis Y, et al. (2003) The Sturtian 'snowball' glaciation: Fire and ice. *Earth Planet Sci Lett* 6648:1–12.
60. Li ZX, et al. (2008) Assembly, configuration, and break-up history of Rodinia: A synthesis. *Precambrian Res* 160(1-2):179–210.
61. Ravizza G, Peucker-Ehrenbrink B (2003) Chemostratigraphic evidence of Deccan volcanism from the marine osmium isotope record. *Science* 302(5649):1392–1395.
62. Turgeon SC, Creaser RA (2008) Cretaceous oceanic anoxic event 2 triggered by a massive magmatic episode. *Nature* 454(7202):323–326.
63. Kent DV, Muttoni G (2013) Modulation of Late Cretaceous and Cenozoic climate by variable drawdown of atmospheric pCO_2 from weathering of basaltic provinces on continents drifting through the equatorial humid belt. *Climates of the Past.* 9: 525–546.
64. Shields G (2005) Neoproterozoic cap carbonates: A critical appraisal of existing models and the plumeworld hypothesis. *Terra Nova* 17(4):299–310.
65. Hoffman PF, et al. (2007) Are basal Ediacaran (635 Ma) post-glacial "cap dolostones" diachronous? *Earth Planet Sci Lett* 258:114–131.
66. Jacobsen S, Kaufman AJ (1999) The Sr, C, and O isotopic evolution of Neoproterozoic seawater. *Chem Geol* 161:37–57.
67. Le Hir G, Ramstein G, Donnadieu Y, Godderis Y (2008) Scenario for the evolution of atmospheric pCO2 during a snowball Earth. *Geology* 36:47–50.
68. Higgins JA, Schrag DP (2003) Aftermath of a snowball Earth. *Geophysics, Geochemistry. Geosystems* 4:1–20.
69. Yoshioka H, Asahara Y, Tojo B, Kawakami S (2003) Systematic variations in C and Sr isotopes and elemental concentrations in Neoproterozoic carbonates in Namibia: Implications for a glacial to interglacial transition. *Precambrian Res* 124:69–85.
70. Shields G, Brasier MD, Stille P, Dorjnamjaa D (2002) Factors contributing to high $\delta^{13}C$ values in Cryogenian limestones of western Mongolia. *Earth Planet Sci Lett* 196: 99–111.
71. Mills B, Watson AJ, Goldblatt C, Boyle RA, Lenton TM (2011) Timing of Neoproterozoic glaciations linked to transport-limited global weathering. *Nat Geosci* 4: 861–864.
72. Planavsky NJ, et al. (2010) The evolution of the marine phosphate reservoir. *Nature* 467(7319):1088–1090.

Supporting Information

Rooney et al. 10.1073/pnas.1317266110

SI Materials and Methods

Sample Selection and Preparation. The Coppercap Formation begins with ~90 m of interbedded red siltstone and tan evaporitic and cupriferous algal limestone in seven sequences referred to as the transition zone (unit CP1). The transition zone is followed by a transgression and deposition of >100 m of gray limey mudstone with relatively low carbonate content (units CP2 and CP3, average 63 wt% carbonate; Table S1) that we refer to herein as marl (Fig. 2). These strata are succeeded by ~150 m of graded beds of limestone alternating between lime mudstone dominated and grainstone dominated (units CP4 and CP5) intervals. The copper deposits formed from the reduction of sulfate-rich brines containing dissolved copper that migrated upward and landward during dewatering of the underlying Redstone River Formation.

Both outcrop and drill core samples of the Windermere Supergroup were analyzed. Core 6Y4 was drilled in 1976 near Coates Lake by Shell Exploration Canada. In 1980, R. Lustwerk sampled these cores, and the remaining core was archived by the Geological Survey of Canada, both of which form the bulk of the analyses made herein. Additional samples from outcrop were collected during fieldwork from 2005 to 2011. No major differences were apparent in the chemistry of the core or outcrop samples.

Pilot samples from the cap carbonate of the Twitya Formation were run from section P5C located near Stoneknife River (64° 41′50″N, 129°53′30″W). $\delta^{13}C_{carb,}$ $\delta^{18}O_{carb}$ results and $\delta^{13}C_{org}$ results from section P5C have been reported previously (1–3). A parallel section, F1173, 30 km to the southeast near Mountain River (64°32′04″N, 129°23′42″W) was collected for Re-Os geochronology and $\delta^{13}C_{carb,}$ $\delta^{18}O_{carb}$, Sr, and Os isotope stratigraphy and trace element geochemistry. Although Total Organic Carbon (TOC) was not measured through section F1173, the high TOC values (1–4 wt. %) from P5C serve as a reference (3).

Samples were cut perpendicular to lamination, revealing internal textures. Between 5 and 20 mg of powder were microdrilled from the individual laminations (where visible), with an eye to avoid veining, fractures, and siliciclastic components. Subsequent trace element, $\delta^{13}C_{carb,}$ $\delta^{18}O_{carb}$, and $^{87}Sr/^{86}Sr$ isotopic analyses were performed on aliquots of this powder.

Carbonate Carbon and Oxygen Isotopes. Carbonate $\delta^{13}C$ and $\delta^{18}O$ isotopic data were acquired simultaneously on a VG Optima dual inlet mass spectrometer attached to a VG Isocarb preparation device (Micromass) in the Harvard University Laboratory for Geochemical Oceanography. Approximately 1 mg of sample powder was reacted in a common, purified H_3PO_4 bath at 90 °C. Evolved CO_2 was collected cryogenically and analyzed using an in-house reference gas. External uncertainty (1σ) from standards was better than ±0.1‰ for both $\delta^{13}C$ and $\delta^{18}O$. Samples were calibrated to Vienna Pee-Dee Belemnite (VPDB) using the Carrara marble standard. $\delta^{13}C$ and $\delta^{18}O$ isotopic results are reported in per mil notation of $^{13}C/^{12}C$ and $^{18}O/^{16}O$, respectively, relative to the standard VPDB. Herein we report $\delta^{13}C$ and $\delta^{18}O$ measurements (Table S1).

Organic Carbon Isotopes. Kerogen $\delta^{13}C$ values were analyzed on a Thermo-Finnigan Delta^{plus} XP isotope ratio monitoring mass spectrometer in the Massachusetts Institute of Technology (MIT) Geobiology laboratories. Sedimentary organic matter was concentrated by carbonate removal with 6 N hydrochloric acid at room temperature. Digestion residues were neutralized, dried, and weighed into tin capsules in triplicate. Capsules were combusted in a Fisons (Carlo Erba) NA 1500 elemental analyzer at 1,030 °C that was fitted with a Costech Zero Blank autosampler and coupled to the Delta^{plus} MS. Stable carbon isotope ratios were determined using an external CO_2 standard calibrated to internal reference materials CH-6 sucrose, NBS-22 oil, and acetanilide. Values are reported relative to the VPDB isotopic standard.

Strontium Isotopes. We report 51 unique $^{87}Sr/^{86}Sr$ measurements from the Coppercap Formation and 34 measurements from the Twitya Formation (Table S1). All $^{87}Sr/^{86}Sr$ data were acquired at the MIT Radiogenic Isotope Laboratory of S. A. Bowring. Approximately 10 mg of each powdered algal-laminated carbonate sample was first leached sequentially three to five times for 15–45 min in an ultrasonic bath, in 1.0 mL of 0.2 M ammonium acetate, to remove loosely bound Sr cations. The remaining solid was then washed three times in an ultrasonic bath with 1.0 mL of ultrapure water to remove excess ammonium and suspended clays. Carbonate was reacted for 5 min with 1.0 mL 1.4 M acetic acid, and insoluble residue was removed by centrifuging. This procedure was slightly modified for analysis of the Twitya samples; these were treated with a 1:1 methanol water solution [three cycles of ~15 min each in an ultrasonic bath (4) before the ammonium acetate step, and the final dissolution used 0.5 M acetic acid instead of 1.4 M acid]. These modifications are designed to reduce the impact of layer silicate impurities and postdepositional dolomite on the measured isotopic compositions. Sr was isolated via standard chromatographic techniques using 50-μL columns of EIChroM SR-spec resin. Samples were analyzed by thermal ionization MS (TIMS) on an Isotopx IsoProbe T in dynamic mode, with target intensity of 3V ^{88}Sr. All data were corrected to $^{86}Sr/^{88}Sr = 0.1194$ for internal mass bias. Each analysis represents a minimum of 60 ratio measurements, with internal precision of better than 0.001% (1-σ). Analyses were referenced against national bureau of standards standard reference material (0.710250), with a long-term average of 0.710240 and 2-σ external precision of 0.000014; no bias correction was made.

Re-Os Geochronology. Samples used in this study are classified as dark-gray to black algal-laminated carbonates, although traditionally, the Re-Os geochronometer was used in siliciclastic strata (5). However, recent analytical and geochronology studies have highlighted that the Re-Os system is reliant on the complexation of Re and Os into organic matter and not on the mineralogy of the strata (6–8). Thus, it is not the use of black shales, *sensu stricto,* but rather the preservation of organic matter within the rock that is the fundamental requirement for Re-Os geochronology.

Organic-lean algal-laminated carbonates (TOC = 0.2–0.5 wt.%; Table S1) from the preglacial Coppercap Formation were obtained from core 6Y4 previously used for Sr, C, and O isotope studies (see above). Four samples large enough for Re-Os geochronology were taken over an interval of 21.6~150 m below the Sayunei Formation of the Rapitan Group. A TOC-rich limestone was sampled near Mountain River, less than 2 m above the contact between the Shezal and Twitya Formations across an ~5-m lateral interval (64°32′04″N 129°23′42″W). Pilot Re-Os data (from section P5C) revealed considerable variations in initial $^{187}Os/^{188}Os$ (Os_i) values throughout the Twitya Formation yielding a highly imprecise age of 669 ± 65 Mya (Table S2). This variation in Os_i values required us to sample a thin vertical interval (<20 cm vertical) of the basal Twitya Formation and

a relatively large horizontal sampling spread was used to maximize the possibility of a large spread in $^{187}Re/^{188}Os$ following ref. 9. Weathered surface material was removed from the Twitya outcrop before sampling by digging an ~1-m-deep trench. The Coppercap drill core and Twitya outcrop samples were polished to remove any possible contamination due to drill contact or rock saw before crushing. All samples were air-dried at 60 °C for 12 h with more than 35 g per sample crushed to a powder (30 μm) using a zirconium dish in a shatterbox to homogenize any Re and Os heterogeneity present in the sample (9). The Re and Os isotopic abundances and compositions were determined at Durham University's TOTAL laboratory for source rock geochronology and geochemistry at the Northern Centre for Isotopic and Elemental Tracing (NCIET) following methodology outlined in refs. 10 and 11. The CrO_3-H_2SO_4 digestion method was used as it has been shown to preferentially liberate hydrogenous Re and Os, thus yielding more accurate and precise age determinations (10, 12, 13).

Between 1 and 1.2 g of sample was digested and equilibrated in 10 mL of CrO_3-H_2SO_4 together with a mixed tracer (spike) solution of ^{190}Os and ^{185}Re in carius tubes at 220 °C for 48 h. Rhenium and Os were purified using anion chromatography, solvent extraction ($CHCl_3$), and microdistillation. The purified Re and Os were loaded onto Ni and Pt filaments, respectively, and analyzed using negative TIMS (N-TIMS) (10, 14). During this study, adjustments were made to the Re purification methodology, chiefly the reduction of Re through SO_2 gas was replaced by a procedure of sample dissolution in 5 N NaOH and transferred to acetone before column chromatography. This step also removed the requirement of a single bead clean-up step (15). Isotopic measurements were performed using a Thermo-Electron TRITON mass spectrometer via static Faraday collection for Re and ion counting using a secondary electron multiplier in peak-hopping mode for Os. Total procedural blanks during this study were 9.5 ± 0.06 and 0.09 ± 0.02 pg (1σ SD, n = 3) for Re and Os, respectively, with an average $^{187}Os/^{188}Os$ value of ~0.31 ± 0.03 (n = 3). In-house Re and Os solutions were continuously analyzed during the course of this study at NCIET to ensure and monitor long-term MS reproducibility. The Re solution is made from 99.999% zone-refined Re ribbon and yields an average $^{185}Re/^{187}Re$ value of 0.59818 ± 0.00149 (1 SD, n = 231), which is identical to that of ref. 16. The measured difference in $^{185}Re/^{187}Re$ values for the Re solution and the accepted $^{185}Re/^{187}Re$ value (0.5974) is used to correct the Re sample data (17). The Os isotope reference material used at NCIET is the Durham Romil Osmium Solution (DROsS), which yields a $^{187}Os/^{188}Os$ ratio of 0.10696 ± 0.00052 (1 SD, n = 146) that is identical, within uncertainty, to those reported in ref. 16.

Elemental Re and Os abundances for the Coppercap Formation samples used for geochronology range from 0.2 to 3.0 ppb and 119 to 768 ppt, respectively, with $^{187}Re/^{188}Os$ and $^{187}Os/^{188}Os$ ratios between 8 and 97, and 0.25 and 1.34, respectively (Table S2). The Twitya Formation geochronology samples have comparable Re abundances (0.3–1.7 ppb) but much lower Os abundances (29–43 ppt) and display a much greater range in $^{187}Re/^{188}Os$ and $^{187}Os/^{188}Os$ ratios (39–514 and 0.97–6.20, respectively; Table S2). For the Os isotope stratigraphy work, elemental Re abundances for the Coppercap and Twitya Formations range from 0.2 to 6.3 and 0.4 to 2.8 ppb, respectively, with Os abundances ranging from 21 to 768 and 12 to 44 ppt, respectively (Tables S3 and S4). The Coppercap Formation Os isotope stratigraphy samples have $^{187}Re/^{188}Os$ and $^{187}Os/^{188}Os$ ratios varying from 8 to 199 and 0.25 to 2.68, respectively, with a larger range seen in the $^{187}Re/^{188}Os$ and $^{187}Os/^{188}Os$ ratios of the Twitya Formation samples: 211–974 and 3.14–11.00, respectively. Regression of the isotopic composition data was performed using the program Isoplot V.4.15 using 2σ uncertainties for $^{187}Re/^{188}Os$ and $^{187}Os/^{188}Os$ and the error correlation function (rho) and a λ ^{187}Re constant of 1.666×10^{-11} a^{-1} (9, 18, 19).

The Re and Os abundances for the Twitya Formation are comparable to that of average continental crust (0.2–2 ppb Re and 30–50 ppt Os) (20, 21) and slightly more elevated for samples from the Coppercap Formation. Regression of the Re-Os isotope data for the Coppercap Formation yields a model 1 age of 732.2 ± 3.9 (4.7) Mya {n = 4, mean square of weighted deviates (MSWD) = 1.9, bracketed uncertainty includes the 0.35% uncertainty in the ^{187}Re decay constant, 2σ uncertainties, initial $^{187}Os/^{188}Os$ [Os_i] = 0.15 ± 0.002; Fig. 3*A*}. The Re-Os isotope data for the Twitya Formation yields a model 1 age of 662.4 ± 3.9 (4.6) Mya (n = 7, MSWD = 1.8, Os_i = 0.54 ± 0.01; Fig. 3*B*).

Calculation of Seawater Os and Sr Isotope Compositions. The schematic ~732 Mya continental weathering inputs of Fig. 5*B* are shown with a continental $^{87}Sr/^{86}Sr$ isotope composition (α) where f_{JC} is the juvenile crust fraction with a Sr isotope composition of 0.7035 and f_{CC} is the upper continental crust fraction with a Sr isotope composition of 0.7120, and $f_{JC} >> f_{CC}$. The $^{187}Os/^{188}Os$ isotope composition (β) is a combination of f_{JC} (juvenile crust fraction with an Os isotope composition of 0.124) and the continental crust composition is calculated via $Os_i = Os_{TC} - \{^{187}Re/^{188}Os_{CC} \times [\exp(1.666 \times 10^{-11} \times F_A) - 1]\}$, where Os_{TC} is the modern-day $^{187}Os/^{188}Os$ of upper continental crust (1.54) from ref. 20, $^{187}Re/^{188}Os_{CC}$ is the $^{187}Re/^{188}Os$ isotope composition of the continental crust (20), and F_A is the age of the formation in Mya. In Fig. 5*C*, ~660 Mya postglacial weathering fluxes where the continental $^{87}Sr/^{86}Sr$ isotope composition (γ) is calculated as in Fig. 5*B*, but $f_{JC} << f_{CC}$. The $^{187}Os/^{188}Os$ isotope composition 662 Mya (ζ) is calculated as in Fig. 5*B*, but f_{CC} = 1.16. The cosmogenic Os flux is assumed to be constant throughout the Cryogenian. Once mixing is established, seawater becomes increasingly radiogenic.

1. Hoffman PF, Schrag DP (2002) The snowball Earth hypothesis: Testing the limits of global change. *Terra Nova* 14(3):129–155.
2. Macdonald FA, et al. (2010) Calibrating the cryogenian. *Science* 327(5970):1241–1243.
3. Johnston DT, Macdonald FA, Gill BC, Hoffman PF, Schrag DP (2012) Uncovering the Neoproterozoic carbon cycle. *Nature* 483(7389):320–323.
4. McArthur J, et al. (2006) A revised Pliocene record for marine-$^{87}Sr/^{86}Sr$ used to date an interglacial event recorded in the Cockburn Island Formation, Antarctic Peninsula. *Palaeogeogr Palaeoclimatol Palaeoecol* 242(1):126–136.
5. Ravizza G, Turekian KK (1989) Application of the ^{187}Re-^{187}Os system to black shale geochronometry. *Geochim Cosmochim Acta* 53:3257–3262.
6. Cumming VM, Selby D, Lillis PG (2012) Re-Os geochronology of the lacustrine Green River Formation: Insights into direct dating of lacustrine successions, Re-Os systematics and paleocontinental weathering. *Earth Planet Sci Lett* 359: 194–205.
7. Rooney AD, Selby D, Lewan MD, Lillis PG, Houzay J-P (2012) Evaluating Re-Os systematics in organic-rich sedimentary rocks in response to petroleum generation using hydrous pyrolysis experiments. *Geochim Cosmochim Acta* 77:225–291.
8. Selby D, Mutterlose J, Condon DJ (2009) U-Pb and Re-Os geochronology of the Aptian/Albian and Cennomanian/Turonian stage boundaries: Implications for timescale calibration, osmium isotope seawater composition and Re-Os systematics in organic-rich sediments. *Chem Geol* 265:394–409.
9. Kendall BS, Creaser RA, Selby D (2009) ^{187}Re-^{188}Os geochronology of Precambrian organic-rich sedimentary rocks. *Geol Soc Lond Spec Publ* 326:85–107.
10. Selby D, Creaser RA (2003) Re-Os geochronology of organic-rich sediments: An evaluation of organic matter analysis methods. *Chem Geol* 200:225–240.
11. Selby D (2007) Direct Rhenium-Osmium age of the Oxfordian-Kimmeridgian boundary, Staffin bay, Isle of Skye, U.K., and the late Jurassic time scale. *Norweigian J Geol* 87:291–299.
12. Rooney AD, Chew DM, Selby D (2011) Re-Os geochronology of the Neoproterozoic-Cambrian Dalradian Supergroup of Scotland and Ireland: Implications for Neoproterozoic stratigraphy, glaciation and Re-Os systematics. *Precambrian Res* 185: 202–214.
13. Kendall BS, Creaser RA, Ross GM, Selby D (2004) Constraints on the timing of Marinoan "Snowball Earth" glaciation by ^{187}Re-^{188}Os dating of a Neoproterozoic post-glacial black shale in Western Canada. *Earth Planet Sci Lett* 222:729–740.
14. Selby D, Creaser RA, Stein HJ, Markey RJ, Hannah JL (2007) Assessment of the ^{187}Re decay constant by cross calibration of Re-Os molybdenite and U-Pb zircon chronometers in magmatic ore systems. *Geochim Cosmochim Acta* 71(8):1999–2013.

15. Cumming VM, Poulton SW, Rooney AD, Selby D (2013) Anoxia in the terrestrial environment during the late Mesoproterozoic. *Geology* 41(5):583–586.
16. Rooney AD, Selby D, Houzay J-P, Renne PR (2010) Re-Os geochronology of a Mesoproterozoic sedimentary succession, Taoudeni basin, Mauritania: Implications for basin-wide correlations and Re-Os organic-rich sediments systematics. *Earth Planet Sci Lett* 289:486–496.
17. Granmlich JW, Murphy TJ, Garner EL, Shields WR (1973) Absolute isotopic abundance ratio and atomic weight of a reference sample of rhenium. *J Res Natl Bur Stand, A Phys Chem* 77A:691–698.
18. Ludwig KR (2011) *User's Manual for Isoplot 4.15: A Geochronological Toolkit for Microsoft Excel* (Berkeley Geochronology Center), Vol 4, 1–70.
19. Ludwig KR (1980) Calculation of uncertainties of U-Pb isotope data. *Earth Planet Sci Lett* 46:212–220.
20. Peucker-Ehrenbrink B, Ravizza G (2000) The marine osmium isotope record. *Terra Nova* 12:205–219.
21. Peucker-Ehrenbrink B, Jahn BM (2001) Rhenium-osmium isotope systematics and platinum group element concentrations: Loess and the upper continental crust. *Geochem Geophys Geosyst* 2(1061).

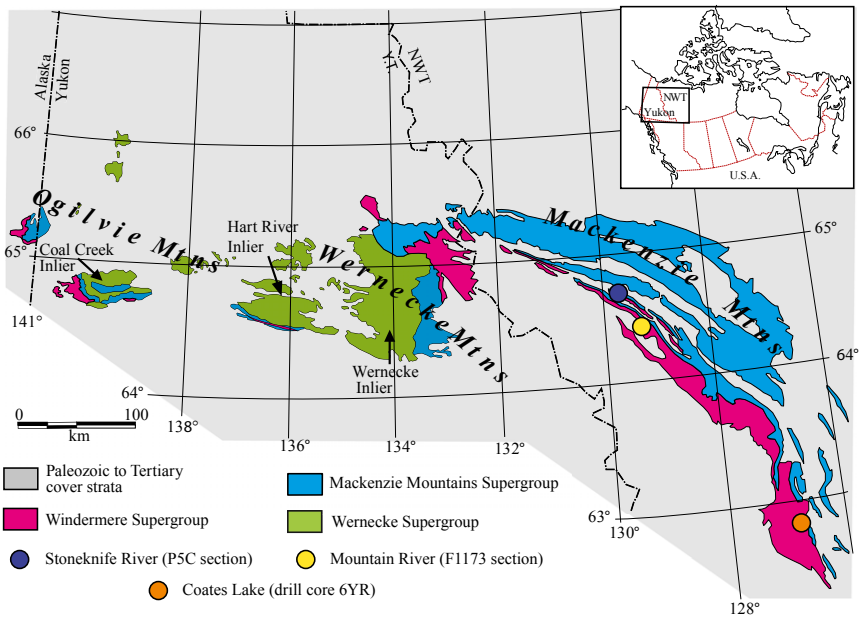

Fig. S1. Location map of study area (*Inset*) and Proterozoic inliers of the Ogilvie, Wernecke, and Mackenzie Mountains, modified from ref. 1.

1. Abbott G (1997) Geology of the Upper Hart River Area, Eastern Ogilvie Mountains, Yukon Territory (116A/10, 116A/11). *Exploration Geol Serv Div Yukon Region Bull* 9:1–76.

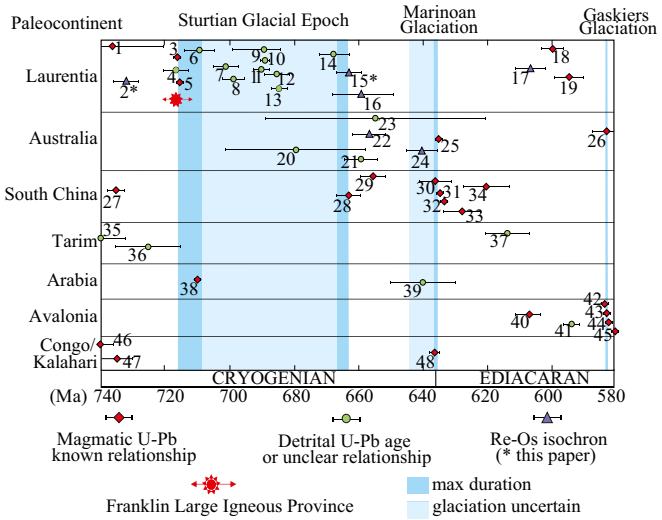

Fig. S2. Compilation of geochronological constraints for Neoproterozoic glaciogenic strata. Further details of the geochronology data and references can be found in Table S6.

Table S1. TOC, carbon, strontium, oxygen isotope, and trace element data for sections of Coppercap and Twitya formations

Rapitan	Sample	Height in m (from base of CC)	Lithology	TOC (wt %)	δ^{13}Ccarb ‰ (VPDB)	Δ^{18}O ‰ (VPDB)	$^{87}Sr/^{86}Sr$	δ^{13}C org ‰ (VPDB)	C Epsilon ‰	Sr (ppm)	Mn (ppm)	Mn/Sr	% CARB	Rb/Sr	Mg/Ca
6YR	76	421.2	gy gs wacke	0.02	2.70	−10.95	0.71021	−36.39	39.09	—	—	—	—	—	—
6YR	77	416.7	diamictite	—	3.68	−10.35	0.71050	—	—	704	4,486	6.372	24.7	0.0240	0.07866
6YR	78	416.6	gy microbial	—	4.43	−10.79	0.70987	—	—	344	1,404	4.080	81.4	0.0101	0.06254
6YR	79	413.7	gy gs	0.01	3.65	−8.64	0.70981	−37.02	40.67	366	1,232	3.365	54.3	0.0052	0.18743
6YR	80	408.2	gy micrite	0.01	5.70	−11.45	0.70841	−25.72	31.42	295	102	0.345	100.1	0.0021	0.00726
6YR	81	405.2	wht brecc dol	—	6.10	−15.15	0.70762	—	—	204	152	0.746	81.5	0.0023	0.00338
6YR	82	402.4	wht brecc dol	—	6.08	−15.88	0.70714	—	—	—	—	—	—	—	—
6YR	83	396.7	wht brecc dol	—	−7.30	−6.41	0.70662	—	—	—	—	—	—	—	—
6YR	84	393.5	dgy gs wacke	0.03	3.69	−4.37	0.70665	−22.83	26.53	1,428	83	0.058	82.5	0.0006	0.18079
6YR	85	379.9	dgy micrite	0.04	6.28	−2.60	0.70667	−20.96	27.24	1,583	50	0.032	76.9	0.0003	0.60862
6YR	86	376.0	dgy micrite	—	5.35	−4.13	0.70668	—	—	1,957	74	0.038	80.5	0.0003	0.19336
6YR	87	374.7	gy gs	0.01	6.72	−4.43	0.70667	−26.89	33.61	—	—	—	—	—	—
6YR	88	368.9	gy gs	—	6.46	−5.26	0.70665	—	—	1,866	95	0.051	68.4	0.0002	0.18952
6YR	89	363.4	gy gs, ev	0.07	5.76	−4.90	0.70657	−31.03	36.79	—	—	—	—	—	—
6YR	90	358.2	dgy micrite	—	5.72	−5.12	0.70664	—	—	1,489	374	0.251	95.6	0.0003	0.03695
6YR	91	353.1	dgy micrite	0.04	7.04	−7.05	0.70653	−18.04	25.09	695	40	0.058	101.1	0.0005	0.00788
6YR	92	347.2	dgy micrite	0.09	5.30	−5.45	0.70667	−22.38	27.67	902	173	0.192	98.0	0.0007	0.05230
6YR	93	341.8	dgy micrite	—	5.08	−5.63	0.70666	—	—	973	118	0.121	98.3	0.0011	0.09666
6YR	94	337.2	dgy micrite	—	6.53	−3.93	0.70651	—	—	807	51	0.063	99.9	0.0005	0.00909
6YR	95	331.2	dgy micrite	0.08	6.59	−3.66	0.70649	−20.53	27.12	1,117	51	0.046	93.9	0.0003	0.00895
6YR	96	325.5	dgy microbial	—	6.33	−3.52	0.70650	—	—	1,267	74	0.058	98.1	0.0009	0.01123
6YR	97	321.2	dgy micrite	0.08	6.15	−4.33	0.70648	−20.55	26.70	1,016	70	0.068	98.8	0.0004	0.01024
6YR	98	315.2	dgy gs wacke	—	4.95	−4.13	0.70650	—	—	1,355	109	0.080	98.3	0.0006	0.01337
6YR	99	311.7	dgy micrite	0.06	4.72	−4.44	0.70648	−22.54	27.26	982	59	0.060	99.9	0.0004	0.01807
6YR	100	305.2	dgy gs	0.05	3.30	−5.30	0.70659	−25.65	28.95	1,205	67	0.056	98.7	0.0003	0.02124
6YR	101	299.2	gy gs	0.11	4.42	−4.27	0.70660	−25.88	30.30	2,048	99	0.048	86.9	0.0012	0.04859
6YR	102	292.0	dgy micrite	0.23	2.64	−3.53	0.70668	−24.16	26.80	1,148	709	0.618	50.2	0.0081	0.41265
6YR	103	284.2	dgy gs	—	2.48	−3.74	0.70674	—	—	1,166	157	0.134	50.7	0.0023	0.12620
6YR	104	277.2	dgy micrite	0.23	2.98	−4.04	0.70669	−25.82	28.80	828	144	0.175	89.8	0.0035	0.14382
6YR	105	268.7	dgy micrite	0.48	2.00	−3.98	0.70691	−26.92	28.92	1,189	103	0.086	89.7	0.0017	0.05358
6YR	106	262.6	dgy micrite	0.36	0.41	−2.79	0.70713	−25.67	26.08	772	347	0.449	83.3	0.0056	0.53384
6YR	107	255.2	dgy micrite	—	0.71	−4.36	0.70704	—	—	1,187	104	0.088	59.1	0.0022	0.10019
6YR	108	249.9	gy gs	0.08	0.71	−6.76	0.70706	−29.31	30.02	1,142	25	0.022	84.3	0.0012	0.05783
6YR	109	242.8	gy gs	—	−1.53	−5.30	0.70683	—	—	1,699	115	0.068	94.3	0.0005	0.55264
6YR	110	235.7	gy gs	0.03	0.29	−3.77	0.70691	−28.75	29.04	1,446	96	0.067	60.1	0.0005	0.58983
6YR	111	229.8	dgy gs	—	0.09	−4.73	0.70751	—	—	684	68	0.099	50.2	0.0011	0.11193
6YR	112	222.5	gy microbial	0.57	−0.86	−5.94	0.70781	−30.06	29.20	—	—	—	—	—	—
6YR	113	217.0	gy gs	0.30	−2.37	−2.90	0.71107	−31.16	28.79	251	720	2.872	95.1	0.0574	0.67578
6YR	114	208.5	dgy micrite	0.45	−3.39	−6.92	0.70939	−33.38	29.99	—	—	—	—	—	—
6YR	115	201.8	dgy microbial	0.08	−2.19	−4.85	0.71457	−28.87	26.67	—	—	—	—	—	—
6YR	116	194.8	dgy micrite	—	−4.54	−3.77	0.70969	—	—	287	1,184	4.119	42.3	0.0310	0.66623
6YR	117	188.2	dgy micrite	1.39	−4.29	−5.58	0.70644	−31.88	27.59	327	824	2.523	51.5	0.0313	0.32804
6YR	118	180.7	dgy micrite	0.17	−5.32	−7.07	0.71280	−30.94	25.62	714	709	0.992	15.1	0.0043	0.06225

Table S1. Cont.

Rapitan	Sample	Height in m (from base of CC)	Lithology	TOC (wt %)	δ^{13}Ccarb ‰ (VPDB)	Δ^{18}O ‰ (VPDB)	$^{87}Sr/^{86}Sr$	δ^{13}C org ‰ (VPDB)	C Epsilon ‰	Sr (ppm)	Mn (ppm)	Mn/Sr	% CARB	Rb/Sr	Mg/Ca
6YR	119	173.2	dgy micrite	—	−3.28	−4.66	0.71352	—	—	—	—	—	—	—	—
6YR	120	168.1	dgy wacke	0.11	−5.02	−6.20	0.70787	−32.34	27.32	888	1,110	1.249	57.2	0.0015	0.21395
6YR	122	152.5	dgy micrite	—	−4.87	−4.90	0.71289	—	—	198	1,788	9.037	61.1	0.0462	0.77903
6YR	123	145.1	dgy micrite	0.17	−4.94	−5.58	0.71324	−31.80	26.86	—	—	—	—	—	—
6YR	125	97.5	gy micrite	0.11	−6.09	−6.17	0.71266	−32.05	25.96	341	1,514	4.441		0.0810	0.31223
6YR	128	99.4	gy micrite	0.26	−4.42	−4.70	0.71688	−31.97	27.55	157	1,652	10.508	37.3	0.0741	0.60216
6YR	129	124.1	gy micrite	0.09	−3.65	−5.01	0.71550	−31.48	27.83	636	179	0.281	79.3	0.0038	0.08526
6YR	130	131.2	gy micrite	0.11	−5.10	−4.74	0.71178	−31.49	26.39	—	—	—	27.2	—	—

Twitya	Sample	Height in m (from contact with Shezal)	Lithology	TOC (wt %)	δ^{13}Ccarb ‰ (VPDB)	Δ^{18}O ‰ (VPDB)	$^{87}Sr/^{86}Sr$	δ^{13}C org ‰ (VPDB)	C Epsilon ‰	Sr (ppm)	Mn (ppm)	Mn/Sr	% CARB	Rb/Sr	Mg/Ca
F1173	0.1	0.1	dgy lime micrite	—	−2.10	−8.40	0.70693	—	—	641	468	0.701	96.1	—	0.01235
F1173	0.5	0.5	dgy lime micrite	—	−2.69	−8.66	0.70751	—	—	—	—	—	—	—	—
F1173	1.0	1.0	dgy lime micrite	—	−2.47	−8.56	0.70690	—	—	—	—	—	—	—	—
F1173	1.6	1.6	dgy lime micrite	—	−0.95	−8.89	0.70686	—	—	—	—	—	—	—	—
F1173	2.0	2.0	dgy lime micrite	—	−1.50	−6.92	0.70678	—	—	—	—	—	—	—	—
F1173	2.6	2.6	dgy lime micrite	—	−0.94	−8.53	0.70681	—	—	—	—	—	—	—	—
F1173	3.1	3.1	dgy lime micrite	—	−0.66	−8.41	0.70672	—	—	2,763	176	0.062	98.0	—	0.01235
F1173	3.0	3.0	dgy lime micrite	—	−0.89	−8.73	—	—	—	—	—	—	—	—	—
F1173	3.7	3.7	dgy lime micrite	—	—	—	0.70675	—	—	—	—	—	—	—	—
F1173	4.3	4.3	dgy lime micrite	—	−0.74	−8.77	—	—	—	—	—	—	—	—	—
F1173	4.9	4.9	dgy lime micrite	—	−0.65	−8.80	0.70682	—	—	—	—	—	—	—	—
F1173	5.5	5.5	dgy lime micrite	—	−0.50	−8.78	0.70681	—	—	—	—	—	—	—	—
F1173	6.0	6.0	dgy lime micrite	—	−0.78	−9.03	0.70680	—	—	2,825	439	0.149	96.0	—	0.03005
F1173	6.5	6.5	dgy lime micrite	—	−0.59	−8.83	—	—	—	—	—	—	—	—	—
F1173	7.0	7.0	dgy lime micrite	—	−0.67	−8.90	—	—	—	—	—	—	—	—	—
F1173	7.5	7.5	dgy lime micrite	—	−0.92	−8.60	0.70676	—	—	3,345	209	0.061	98.0	—	0.01344
F1173	8.0	8.0	dgy lime micrite	—	−0.90	−9.25	0.70676	—	—	3,052	210	0.069	100.0	—	0.01487
F1173	8.5	8.5	dgy lime micrite	—	−0.90	−9.03	—	—	—	—	—	—	—	—	—
F1173	9.0	9.0	dgy lime micrite	—	−0.93	−9.08	—	—	—	—	—	—	—	—	—
F1173	9.5	9.5	dgy lime micrite	—	−0.98	−9.07	0.70674	—	—	3,808	137	0.035	98.0	—	0.01118
F1173	10.0	10.0	dgy lime micrite	—	−0.87	−9.26	—	—	—	—	—	—	—	—	—
F1173	10.5	10.5	dgy lime micrite	—	−0.51	−9.25	0.70682	—	—	2,248	761	0.332	98.0	—	0.03263
F1173	11.0	11.0	dgy lime micrite	—	−0.34	−8.80	0.70685	—	—	2,082	468	0.225	100.0	—	0.02748
F1173	11.5	11.5	dgy lime micrite	—	−0.25	−8.82	0.70677	—	—	3,007	597	0.198	100.0	—	0.03911
F1173	12.0	12.0	dgy lime micrite	—	−0.55	−8.81	0.70681	—	—	2,761	579	0.210	100.0	—	0.11319
F1173	12.5	12.5	dgy lime micrite	—	−0.62	−8.31	—	—	—	—	—	—	—	—	—
F1173	13.0	13.0	dgy lime micrite	—	−0.57	−9.16	—	—	—	—	—	—	—	—	—
F1173	13.5	13.5	dgy lime micrite	—	−0.28	−8.81	—	—	—	—	—	—	—	—	—
F1173	14.0	14.0	dgy lime micrite	—	−0.33	−7.93	0.70676	—	—	3,512	1,220	0.347	100.0	—	0.02686
F1173	14.5	14.5	dgy lime micrite	—	−0.16	−8.78	0.70679	—	—	2,240	733	0.327	100.0	—	0.03638
F1173	15.0	15.0	dgy lime micrite	—	−0.26	−8.46	—	—	—	—	—	—	—	—	—

Table S1. Cont.

Rapitan	Sample	Height in m (from base of CC)	Lithology	TOC (wt %)	δ^{13}Ccarb ‰ (VPDB)	Δ^{18}O ‰ (VPDB)	$^{87}Sr/^{86}Sr$	δ^{13}C org ‰ (VPDB)	C Epsilon ‰	Sr (ppm)	Mn (ppm)	Mn/Sr	% CARB	Rb/Sr	Mg/Ca
F1173	15.5	15.5	dgy lime micrite	—	−0.18	−9.03	—	—	—	—	—	—	—	—	—
F1173	16.0	16.0	dgy lime micrite	—	−0.77	−9.00	—	—	—	—	—	—	—	—	—
F1173	16.5	16.5	dgy lime micrite	—	−0.22	−9.21	0.70681	—	—	3,084	663	0.206	95.9	—	0.03936
F1173	17.0	17.0	dgy lime micrite	—	−0.36	−8.50	0.70692	—	—	2,924	905	0.297	96.0	—	0.10666
F1173	17.5	17.5	dgy lime micrite	—	−0.24	−6.51	0.70677	—	—	3,340	1,319	0.387	98.0	—	0.02427
F1173	18.0	18.0	dgy lime micrite	—	−0.38	−7.56	—	—	—	—	—	—	—	—	—
F1173	18.5	18.5	dgy lime micrite	—	−0.20	−9.15	—	—	—	—	—	—	—	—	—
F1173	19.0	19.0	dgy lime micrite	—	0.04	−9.02	0.70679	—	—	2,372	509	0.202	94.1	—	0.03203
F1173	19.5	19.5	dgy lime micrite	—	0.04	−9.25	0.70683	—	—	2,594	615	0.223	94.1	—	0.03571
F1173	20.0	20.0	dgy lime micrite	—	−0.09	−8.53	—	—	—					—	—
F1173	20.5	20.5	dgy lime micrite	—	−0.11	−9.23	0.70684	—	—	3,240	662	0.200	98.0	—	0.02726
F1173	21.0	21.0	dgy lime micrite	—	−0.15	−9.81	0.70692	—	—	2,062	538	0.250	96.0	—	0.02899
F1173	21.5	21.5	dgy lime micrite	—	−0.24	−8.66	—	—	—					—	—
F1173	22.0	22.0	dgy lime micrite	—	−0.03	−8.92	0.70686	—	—	2,671	735	0.243	88.2	—	0.06239
F1173	22.5	22.5	dgy lime micrite	—	0.01	−9.01	—	—	—	—	—	—	—	—	—
F1173	23.0	23.0	dgy lime micrite	—	−0.60	−9.10	0.70681	—	—	3,470	593	0.161	94.1	—	0.05661
F1173	23.5	23.5	dgy lime micrite	—	−1.50	−10.48	—	—	—	—	—	—	—	—	—
F1173	24.5	24.5	dgy lime micrite	—	−0.01	−8.79	—	—	—	—	—	—	—	—	—
F1173	25.0	25.0	dgy lime micrite	—	0.25	−8.62	—	—	—	—	—	—	—	—	—
F1173	25.5	25.5	dgy lime micrite	—	0.38	−9.14	0.70683	—	—	2,675	381	0.140	98.0	—	0.03017
F1173	26.0	26.0	dgy lime micrite	—	0.34	−9.20	—	—	—	—	—	—	—	—	—
F1173	26.5	26.5	dgy lime micrite	—	0.09	−9.17	—	—	—	—	—	—	—	—	—
F1173	27.0	27.0	dgy lime micrite	—	0.73	−5.28	0.70684	—	—	1,513	703	0.446	96.1	—	0.09318
F1173	27.5	27.5	dgy lime micrite	—	−0.68	−8.46	0.70687	—	—	2,898	455	0.154	98.0	—	0.11465
F1173	28.0	28.0	dgy lime micrite	—	−0.23	−8.73	0.70701	—	—	2,283	483	0.181	85.7	—	0.14863
F1173	28.5	28.5	dgy lime micrite	—	0.29	−7.65	—	—	—	—	—	—	—	—	—
F1173	29.5	29.5	dgy lime micrite	—	−0.02	−9.85	0.70692	—	—	2,454	300	0.103	84.0	—	0.04424
F1173	30.0	30.0	dgy lime micrite	—	0.67	−9.90	—	—	—	—	—	—	—	—	—

brecc, brecciated; dol, dolomite; (d)gy, (dark)gray; ev, evaporite; gs, grainstone; wacke, wackestone; wht, white.

Table S2. Re and Os abundance and isotopic composition for the Coppercap and Twitya formations

Sample	Re (ppb)	±	Os (ppt)	±	$^{187}Re/^{188}Os$	±	$^{187}Os/^{188}Os$	±	rho*	Osi†
Coppercap Formation										
103	2.531	0.008	768.4	2.1	16.321	0.10	0.3457	0.0018	0.5270	0.1454
104	0.201	0.001	119.3	0.5	8.254	0.08	0.2448	0.0028	0.6072	0.1436
105	2.551	0.009	199.0	0.8	68.678	0.35	0.9850	0.0052	0.5227	0.1423
106	2.998	0.010	172.6	0.9	96.947	0.62	1.3383	0.0103	0.6030	0.1488
Twitya Formation										
TW1-A	0.295	0.001	40.3	0.2	39.139	0.34	0.9687	0.0116	0.6268	0.535
TW1-B	1.269	0.004	30.8	0.3	294.679	2.56	3.8276	0.0391	0.7331	0.560
TW1-C	1.726	0.006	29.0	0.3	514.190	5.70	6.2025	0.0830	0.7585	0.561
TW1-D	1.273	0.004	37.0	0.3	229.301	2.22	3.0721	0.0377	0.6992	0.529
TW1-E	1.080	0.010	32.3	0.3	220.303	2.93	2.9542	0.0370	0.5295	0.511
TW1-F	1.103	0.004	33.7	0.3	215.500	2.19	2.9251	0.0373	0.7182	0.535
TW1-G	1.489	0.005	43.2	0.4	230.638	2.17	3.1113	0.0374	0.6900	0.554
P5c Pilot study data										
P5c 1.4	0.769	0.003	16.1	0.2	368.536	3.30	4.7483	0.0557	0.6536	0.705
Pc5 1.7	0.657	0.002	15.5	0.1	308.627	2.73	4.0689	0.0469	0.6529	0.683
P5c 2.0	0.559	0.002	13.5	0.1	302.701	2.73	4.0868	0.0483	0.6519	0.766
P5c 2.5	1.050	0.004	22.6	0.3	358.175	5.00	4.7418	0.0899	0.6828	0.812
P5c 3.0	0.383	0.001	9.8	0.1	283.465	2.60	4.0070	0.0473	0.6422	0.897
P5c 3.5	0.486	0.002	13.1	0.1	254.034	2.30	3.3830	0.0391	0.6405	0.596
P5c 4.0	0.524	0.002	12.1	0.1	323.905	2.95	4.3451	0.0518	0.6512	0.791
P5c 5.9	1.231	0.004	24.5	0.3	405.603	5.68	5.3006	0.1020	0.6875	0.850
P5c 6.5	1.139	0.005	22.0	0.3	422.203	7.10	5.4142	0.1239	0.6818	0.782
P5c 7.0	0.408	0.001	13.0	0.2	211.206	3.48	3.1370	0.0714	0.6929	0.820
P5c 7.5	1.214	0.004	28.2	0.4	324.681	5.38	4.4472	0.1022	0.6925	0.885

Uncertainties are given as 2σ for $^{187}Re/^{188}Os$ and $^{187}Os/^{188}Os$ and ^{192}Os. The uncertainty includes the 2 SE uncertainty for mass spectrometer analysis plus uncertainties for Os blank abundance and isotopic composition. P5c Pilot study data were collected 2010.
*Rho is the associated error correlation (1).
†Os_i = initial $^{187}Os/^{188}Os$ isotope ratio calculated at 732 Mya (Coppercap Formation) and 662 Mya (Twitya Formation).

1. Ludwig KR (1980) Calculation of uncertainties of U-Pb isotope data. *Earth Planet Sci Lett* 46:212–220.

Table S3. Re and Os abundance and isotopic composition for Coppercap Formation Os isotope stratigraphy samples

Sample	Height (m) below Sayunei	Re (ppb)	±	Os (ppt)	±	$^{187}Re/^{188}Os$	±	$^{187}Os/^{188}Os$	±	rho*	Osi†
95	85.5	0.3	0.001	21.0	0.3	87.1	1.8	1.19	0.034	0.692	0.117
97	95.5	0.4	0.001	48.0	0.3	38.3	0.4	0.61	0.008	0.591	0.135
98	101.5	0.7	0.003	95.2	0.4	39.5	0.2	0.64	0.005	0.580	0.157
101	117.5	0.4	0.001	98.9	0.5	17.6	0.2	0.38	0.004	0.632	0.161
103	132.5	2.5	0.008	768.4	2.1	16.3	0.1	0.35	0.002	0.527	0.145
104	139.5	0.2	0.001	119.3	0.5	8.3	0.1	0.24	0.003	0.607	0.144
105	148.0	2.6	0.009	199.0	0.8	68.7	0.3	0.98	0.005	0.523	0.142
106	154.1	3.0	0.010	172.6	0.9	96.9	0.6	1.34	0.010	0.603	0.149
107	161.5	1.2	0.004	162.1	0.9	37.0	0.3	0.58	0.007	0.652	0.125
109	173.9	4.4	0.014	271.6	1.8	88.9	0.8	1.21	0.014	0.656	0.122
112	194.2	0.3	0.001	15.0	0.6	99.2	8.0	1.49	0.170	0.707	0.277
114	208.2	6.3	0.020	258.0	1.9	146.4	1.3	1.98	0.023	0.656	0.183
115	214.9	2.0	0.012	182.9	1.2	61.5	0.6	1.24	0.014	0.571	0.483
118	236.0	6.3	0.021	204.1	1.7	199.2	1.7	2.68	0.030	0.656	0.235

Uncertainties are given as 2σ for $^{187}Re/^{188}Os$ and $^{187}Os/^{188}Os$ and ^{192}Os. The uncertainty includes the 2 SE uncertainty for mass spectrometer analysis plus uncertainties for Os blank abundance and isotopic composition.
*Rho is the associated error correlation (1).
†Os_i = initial $^{187}Os/^{188}Os$ isotope ratio calculated 732 Mya.

1. Ludwig KR (1980) Calculation of uncertainties of U-Pb isotope data. *Earth Planet Sci Lett* 46:212–220.

Table S4. Re and Os abundance and isotopic composition for Twitya Formation Os isotope stratigraphy samples

Height (m) from contact with Shezal Formation (F1173)	Re (ppb)	±	Os (ppt)	±	$^{187}Re/^{188}Os$	±	$^{187}Os/^{188}Os$	±	rho*	Osi†
0.1	1.88	0.006	35.7	0.3	470.3	3.9	6.65	0.06	0.835	1.439
0.5	2.28	0.007	39.8	0.4	515.7	5.1	6.77	0.08	0.723	1.050
1.0	1.83	0.006	32.4	0.4	483.9	5.1	6.07	0.08	0.742	0.707
1.6	1.09	0.004	27.3	0.3	285.2	3.1	3.81	0.05	0.726	0.644
2.0	0.65	0.002	16.0	0.2	282.7	3.9	3.59	0.06	0.777	0.453
2.6	0.97	0.003	21.9	0.7	322.1	15.5	4.00	0.28	0.677	0.424
3.1	1.30	0.004	28.9	0.3	338.5	3.6	4.39	0.06	0.730	0.636
3.7	2.00	0.006	43.6	0.3	347.7	2.3	4.51	0.03	0.691	0.652
4.9	1.00	0.003	23.2	0.2	322.4	3.8	4.29	0.06	0.753	0.715
8.5	1.27	0.004	24.8	0.2	406.8	3.6	5.14	0.06	0.658	0.620
15.5	0.59	0.002	17.1	0.1	231.3	2.0	3.06	0.04	0.658	0.498
22.5	0.59	0.002	16.1	0.1	248.3	2.2	3.28	0.04	0.653	0.527

Uncertainties are given as 2σ for $^{187}Re/^{188}Os$ and $^{187}Os/^{188}Os$ and ^{192}Os. For the latter the uncertainty includes the 2 SE uncertainty for mass spectrometer analysis plus uncertainties for Os blank abundance and isotopic composition. F1173 samples collected 2011.
*Rho is the associated error correlation (1).
†Os_i = initial $^{187}Os/^{188}Os$ isotope ratio calculated 662 Mya.

1. Ludwig KR (1980) Calculation of uncertainties of U-Pb isotope data. *Earth Planet Sci Lett* 46:212–220.

Table S5. Re and Os isotopic composition and calculated Osi data for published Rapitan-Sturtian Re-Os geochronology studies

Sample	$^{187}Re/^{188}Os$	±	$^{187}Os/^{188}Os$	±	rho*	Os_i values for published isochron age (Mya) 657[†]	Calculated Os_i values for deglaciation (660 Mya) 660
1a	262.1	1.2	3.72	0.01	0.525	0.832	0.819
1ar	263.4	1.2	3.71	0.01	0.436	0.816	0.803
1b	252.0	1.6	3.59	0.03	0.543	0.821	0.808
2a	304.3	1.5	4.17	0.02	0.596	0.817	0.802
2b	309.8	1.6	4.23	0.02	0.473	0.818	0.802
3	320.0	2.0	4.36	0.03	0.661	0.839	0.822
4a	421.9	2.4	5.47	0.03	0.603	0.830	0.809
4b	405.0	2.0	5.27	0.02	0.479	0.809	0.788
5a	447.2	3.3	5.75	0.04	0.746	0.825	0.803
5ar	444.0	2.7	5.72	0.04	0.625	0.834	0.811
						645[†]	
1	215.7	1.3	3.28	0.02	0.545	0.952	0.897
3	201.1	1.0	3.12	0.01	0.524	0.945	0.894
4	138.6	0.9	2.45	0.02	0.585	0.958	0.923
5	109.5	0.6	2.13	0.01	0.460	0.949	0.922
r	110.8	1.0	2.12	0.03	0.559	0.927	0.899
6	102.3	0.6	2.06	0.01	0.466	0.951	0.925
7	234.0	1.3	3.47	0.02	0.527	0.944	0.885
r	224.8	1.6	3.37	0.03	0.553	0.943	0.886
9	220.2	1.2	3.34	0.02	0.486	0.960	0.905
10	217.2	1.3	3.31	0.02	0.556	0.960	0.905
11	228.8	1.3	3.41	0.02	0.504	0.940	0.883
						647[†]	
a3-4	778.7	5.4	9.37	0.08	0.594	0.933	0.762
a3-4r	649.8	3.8	7.93	0.05	0.577	0.888	0.745
a5	551.2	4.2	6.87	0.06	0.613	0.897	0.776
a6-7	1,010.0	6.2	11.83	0.08	0.597	0.886	0.665
						662.4[‡]	
TW1-A	514.2	5.7	6.20	0.08	0.759	0.497	0.517
TW1-B	220.3	2.9	2.95	0.04	0.529	0.510	0.519
TW1-C	229.3	2.2	3.07	0.04	0.699	0.528	0.537
TW1-D	215.5	2.2	2.93	0.04	0.718	0.534	0.542
TW1-E	39.1	0.3	0.97	0.01	0.627	0.534	0.536
TW1-F	230.6	2.2	3.11	0.04	0.690	0.552	0.561
TW1-G	294.7	2.6	3.83	0.04	0.733	0.558	0.570

Uncertainties are given as 2σ for $^{187}Re/^{188}Os$ and $^{187}Os/^{188}Os$ and ^{192}Os. The uncertainty includes the 2 SE uncertainty for mass spectrometer analysis plus uncertainties for Os blank abundance and isotopic composition. Os_i values calculated using the $\lambda\ ^{187}Re = 1.666 \times 10^{-11}y^{-1}$ (1).

*Rho is the associated error correlation (2).

[†]Kendall et al. 2006.

[‡]This paper.

1. Smoliar MI, Walker RJ, Morgan JW (1996) Re-Os ages of group IIA, IIIA, IVA, and IVB iron meteorites. *Science* 271:1099–1102.
2. Ludwig KR (1980) Calculation of uncertainties of U-Pb isotope data. *Earth Planet Sci Lett* 46:212–220.
3. Kendall BS, Creaser RA, Selby D (2006) Re-Os geochronology of postglacial black shales in Australia:Cconstraints on the timing of "Sturtian" glaciation. *Geology* 34:729–732.

Table S6. Geolochronological age constraints, techniques, and data sources for Fig. S2

Paleocontinent	Age (Mya)	(+)	(–)	Technique	Grains	Relationship to glacial deposit	Number	Reference
Laurentia	736.0	23.0	17.0	U-Pb TIMS	magmatic	below Rapitan	1	(1)
	732.1	3.9	3.9	Re-Os	isochron	below Rapitan	2	This paper
	717.4	0.1	0.1	U-Pb TIMS	magmatic	below Rapitan	3	(2)
	717.0	4.0	4.0	U-Pb TIMS	detrital	within Scout Mountain	4	(3)
	716.5	0.2	0.2	U-Pb TIMS	magmatic	within Rapitan	5	(2)
	709.0	5.0	5.0	U-Pb SHRIMP	magmatic	unknown	6	(3)
	701.0	4.0	4.0	U-Pb SHRIMP	detrital	within Scout Mountain	7	(4)
	699.0	3.0	3.0	U-Pb SHRIMP	magmatic	unknown	8	(5)
	688.9	9.5	6.2	U-Pb TIMS	magmatic	unknown	9	(6)
	687.4	1.3	1.3	U-Pb TIMS	magmatic	unknown	10	(7)
	686.0	4.0	4.0	U-Pb SHRIMP	magmatic	unknown	11	(4)
	685.0	7.0	7.0	U-Pb SHRIMP	magmatic	unknown	12	(8)
	684.0	4.0	4.0	U-Pb SHRIMP	magmatic	unknown	13	(8)
	667.0	5.0	5.0	U-Pb SHRIMP	detrital	within Scout Mountain	14	(3)
	662.4	3.9	3.9	Re-Os	isochron	above Rapitan	15	This paper
	659.6	9.6	9.6	Re-Os	isochron	below Port Askaig	16	(9)
	607.8	4.7	4.7	Re-Os	isochron	above Ice Brook	17	(10)
	601.4	3.7	3.7	U-Pb SHRIMP	magmatic	above Port Askaig	18	(11)
	595.0	4.0	4.0	U-Pb TIMS	magmatic	above Port Askaig	19	(12)
Australia	680.0	23.0	23.0	U-Pb EM	authigenic monazite	between Sturtian and Marinoan	20	(13)
	659.7	5.3	5.3	U-Pb SHRIMP	detrital	within Sturtian	21	(4)
	657.2	5.4	5.4	Re-Os	isochron	above Sturtian below Marinoan	22	(14)
	655.0	34.0	34.0	U-Pb SHRIMP	detrital	below Marinoan	23	(15)
	640.7	4.7	4.7	Re-Os	isochron	above Sturtian	24	(14)
	636.4	0.5	0.5	U-Pb TIMS	magmatic	within Cottons Breccia	25	(16)
	582.0	4.0	4.0	U-Pb SHRIMP	magmatic	below Croles Hill	26	(17)
South China	736.0	2.0	2.0	U-Pb SHRIMP	magmatic	below Chang'an	27	(18)
	663.0	4.0	4.0	U-Pb TIMS	magmatic	below Nantuo above Tiesiao	28	(19)
	654.5	3.8	3.8	U-Pb SHRIMP	magmatic	below Nantuo	29	(20)
	636.3	4.9	4.9	U-Pb SHRIMP	magmatic	within Nantuo	30	(20)
	635.2	0.6	0.6	U-Pb TIMS	magmatic	above Nantuo	31	(21)
	632.5	0.5	0.5	U-Pb TIMS	magmatic	above Nantuo	32	(21)
	628.3	5.8	5.8	U-Pb TIMS	magmatic	above Nantuo	33	(22)
	621.0	7.0	7.0	U-Pb SHRIMP	magmatic	above Nantuo	34	(23)
Tarim	740.0	7.0	7.0	U-Pb SHRIMP	inherited	within Bayisi	35	(24)
	725.0	10.0	10.0	U-Pb SHRIMP	inherited	within Bayisi	36	(24)
	615.0	6.0	6.0	U-Pb SHRIMP	unknown	between Tereeken and Hankalchough	37	(24)
Arabia	711.5	0.3	0.3	U-Pb TIMS	magmatic	within Ghubrah	38	(25)
	640.0	10.0	10.0	U-Pb TIMS	detrital	within Fiq	39	(25)
Avalonia	606.0	3.7	2.9	U-Pb TIMS	magmatic	below Gaskiers	40	(26)
	595.5	2.0	2.0	U-Pb TIMS	detrital	within Squantum	41	(27)
	583.7	0.5	0.5	U-Pb TIMS	magmatic	below Gaskiers	42	(28)
	582.4	0.5	0.5	U-Pb TIMS	magmatic	within Gaskiers	43	(28)
	582.1	0.5	0.5	U-Pb TIMS	magmatic	above Gaskiers	44	(28)
	579.0	0.5	0.5	U-Pb TIMS	magmatic	above Gaskiers	45	(29)
Congo & Kalahari	741.0	6.0	6.0	U-Pb TIMS	magmatic	below Numees	46	(30)
	735.0	5.0	5.0	U-Pb SHRIMP	magmatic	below Kundelungu	47	(31)
	635.5	1.2	1.2	U-Pb TIMS	magmatic	within Ghuab	48	(32)

All age uncertainties are 2σ. EM, electron microprobe; SHRIMP, sensitive high-resolution ion microprobe; TIMS, thermal ionization MS.

1. McDonough MR, Parish RR (1991) Proterozoic gneisses of the Malton Complex, near Valemount, British Columbia: U-Pb ages and Nd isotopic signatures. *Canadian Journal of Earth Sciences* 28:1202–1216.
2. Macdonald FA, et al. (2010) Calibrating the Cryogenian. *Science* 327:1241–1243.
3. Fanning CM, Link PK (2004) U-Pb SHRIMP ages of Neoproterozoic (Sturtian) glaciogenic Pocatello Formation, southeastern Idaho. *Geology* 32:881–884.
4. Fanning CM, Link PK (2008) Age constraints for the Sturtian glaciation: Data from the Adelaide Geosyncline, South Australia and Pocatello Formation Idaho, USA. *Neoproterozoic Extreme Climates and the Origin of Early Metazoan Life, Selwyn Symposium*, eds Gallagher SJ, Wallace MW (Geological Society of Australia, Sydney), pp 57–62.
5. Evans KV, Lund K, Aleinikoff JN, Fanning CM (1997) Shrimp U-Pb age of Late Proterozoic volcanism in central Idaho. *Geological Society of America, Abstracts with Programs* 6: A196.
6. Ferri F, Rees CJ, Nelson JL, Legun AS, (1999) Geology and mineral deposits of the northern Kechika Trough between Gataga River and the 60th parallel. *British Columbia Ministry of Energy and Mines, Bulletin* 107:1–122
7. Condon DJ, Bowring SA (2011) A user's guide to Neoproterozoic geochronology. *Geological Society, London, Memoirs*, 36:135–149.
8. Lund K, Aleinikoff JN, Evans KV, Fanning CM (2003) SHRIMP U-Pb geochronology of Neoproterozoic Windermere Supergroup, central Idaho: Implications for rifting of western Laurentia and synchroneity of Sturtian glacial deposits. *Geological Society of America Bulletin*, 115:349–372.
9. Rooney AD, Chew DM, Selby D (2011) Re-Os geochronology of the Neoproterozoic-Cambrian Dalradian Supergroup of Scotland and Ireland: Implications for Neoproterozoic stratigraphy, glaciation and Re-Os systematics. *Precambrian Research* 185:202–214.
10. Kendall BS, Creaser RA, Ross GM, Selby D (2004) Constraints on the timing of Marinoan "Snowball Earth" glaciation by ^{187}Re-^{188}Os dating of a Neoproterozoic postglacial black shale in Western Canada. *Earth and Planetary Science Letters* 222:729–740.

11. Dempster TJ, et al. (2002) Timing of deposition, orogenesis and glaciation within the Dalradian rocks of Scotland: Constraints from U-Pb zircon ages. *Journal of the Geological Society*, 159:83–94.
12. Halliday AN, Graham CM, Aftalion M, Dymoke P (1989) Short Paper: The depositional age of the Dalradian Supergroup: U-Pb and Sm-Nd isotopic studies of the Tayvallich Volcanics, Scotland. *Journal of the Geological Society*, 146:3–6.
13. Mahan KH, Wernicke BP, Jercinovic MJ (2010) Th–U–total Pb geochronology of authigenic monazite in the Adelaide rift complex, South Australia, and implications for the age of the type Sturtian and Marinoan glacial deposits. *Earth and Planetary Science Letters* 289:76–86.
14. Kendall BS, Creaser RA, Selby D (2006) Re-Os geochronology of postglacial black shales in Australia: constraints on the timing of "Sturtian" glaciation. *Geology* 34:729–732.
15. Ireland TR, Flottmann T, Fanning CM, Gibson GM, Preiss, WV (1998) Development of the early Paleozoic Pacific margin of Gondwana from detrital-zircon ages across the Delamerian orogen. *Geology,* 26:243–246.
16. Calver CR, et al. (2013) Globally synchronous Marinoan deglaciation indicated by U-Pb geochronology of the Cottons Breccia, Tasmania, Australia. *Geology* 41:1127–1130.
17. Calver CR, Black LP, Everard JL, Seymour DB (2004) U-Pb zircon age constraints on late Neoproterozoic glaciation in Tasmania. *Geology* 32:893–896.
18. Gan X, Zhao F, Li H, Tang X, Huang J, (1993) Single zircon U-Pb age of the Banxi Group in Hunan Province. *Abstracts of the Fifth National Symposium on Isotopic Geochronology and Geochemistry* 10–12. Chinese.
19. Zhou C, et al. (2004) New constraints on the ages of Neoproterozoic glaciations in south China. *Geology* 32:437–440.
20. Zhang S, Jiang G, Han Y. (2008) The age of the Nantuo Formation and Nantuo glaciation in South China. *Terra Nova* 20:289–294.
21. Condon D, et al. (2005) U-Pb ages from the neoproterozoic Doushantuo Formation, China. *Science* 308:95–98.
22. Yin CY, et al. (2005) U-Pb zircon age from the base of the Ediacaran Doushantuo Formation in the Yangtze Gorges, South China: Constraint on the age of Marinoan glaciation. *Episodes* 28:48–49.
23. Zhang S, et al. (2005) U-Pb sensitive high–resolution ion microprobe ages from the Doushantuo Formation in south China: Constraints on late Neoproterozoic glaciations. *Geology* 33:473–476.
24. Xu B, et al. (2009) SHRIMP zircon U-Pb age constraints on Neoproterozoic Quruqtagh diamictites in NW China. *Precambrian Research* 168:247–258.
25. Bowring SA, et al. (2007) Geochronologic constraints on the chronostratigraphic framework of the Neoproterozoic Huqf Supergroup, Sultanate of Oman. *American Journal of Science* 307:1097–1145.
26. Krogh TE, Strong DF, O'Brien SJ, Papezik VS (1988) Precise U-Pb zircon dates from the Avalon Terrane in Newfoundland (Canada). *Canadian Journal of Earth Sciences* 25:442–453.
27. Thompson MD, Bowring SA (2000) Age of the Squantum tillite Boston Basin, Massachusetts: U-PB zircon constraints on terminal Neoproterozoic glaciation. *American Journal of Science* 300:630–655.
28. Hoffman PF, Li ZX (2009) A palaeogeographic context for Neoproterozoic glaciation. *Palaeogeography, Palaeoclimatology, Palaeoecology* 277:158–172.
29. Bowring SA, Myrow P, Landing E, Ramezani J, Grotzinger J, (2003) Geochronological constraints on terminal Neoproterozoic events and the rise of metazoans. *Geophysical Research Abstracts* 5:13, 219.
30. Frimmel HE, Klötzli US, Siegfried PR (1996) New Pb-Pb single zircon age constraints on the timing of Neoproterozoic glaciation and continental break–up in Namibia. *The Journal of Geology* 104:459–469.
31. Key RM, et al. (2001) The western arm of the Lufilian Arc in NW Zambia and its potential for copper mineralization. *Journal of African Earth Sciences* 33:503–528.
32. Hoffmann K-H, Condon DJ, Bowring SA, Crowley TJ (2004) U-Pb zircon date from the Neoproterozoic Ghuab Formation, Namibia: Constraints on Marinoan glaciation. *Geology* 32:817–820.